Contrib Mineral Petrol (2005) 149: 627–646
DOI 10.1007/s00410-005-0678-3

ORIGINAL PAPER

V. López Sánchez-Vizcaíno · V. Trommsdorff
M. T. Gómez-Pugnaire · C. J. Garrido · O. Müntener
J. A. D. Connolly

Petrology of titanian clinohumite and olivine at the high-pressure breakdown of antigorite serpentinite to chlorite harzburgite (Almirez Massif, S. Spain)

Received: 4 January 2005 / Accepted: 14 April 2005 / Published online: 20 May 2005

Abstract Rocks of the Cerro del Almirez ultramafic massif (Sierra Nevada, Betic Cordillera, S. Spain) record the high-pressure dehydration of antigorite–olivine serpentinite to form chlorite harzburgite (ol + opx + chl). In the field, these two rock types are separated by a well-defined isograd. Titanian clinohumite (TiCl) and olivine show textural and compositional differences depending on the rock type. OH–TiCl occurs in the serpentinite as disseminated grains and in veins. F–OH–TiCl is observed exclusively in the chlorite harzburgite, where it occurs as porphyroblastic grains and within prograde olivine as irregular and lamellar, planar intergrowths at microscopic and submicroscopic scales. Petrological evidence of partial to complete breakdown of TiCl to olivine + ilmenite is preserved in both rock types. Chlorite harzburgite is characterized by a brown pleochroic olivine with abundantally oriented microscopic to submicroscopic oxide particles. The mean Ti-content of the brown olivine is 144 ppm. The brown olivine preserves TiCl lamellae that sometimes grade into ghost lamellae outlined by the oxide trails. This observation suggests that some of the oxide inclusions in the brown olivine are derived from the breakdown of TiCl intergrowths. Thermodynamic modelling of selected Almirez bulk rock compositions indicates a temperature increase from 635°C to 695°C, at pressures ranging from 1.7 GPa to 2.0 GPa, as the cause for the compositional adjustment of TiCl between the Almirez antigorite serpentinite and chlorite harzburgite. These *P–T* estimates are in good agreement with the sequence of phase relations observed in the field. The computed phase diagrams in conjunction with the geothermal conditions envisaged for different subduction settings indicate that TiCl is stable in the vicinity of the antigorite serpentinite/chlorite harzburgite phase boundary in some subduction settings. In these circumstances, clinohumite–olivine intergrowths in chlorite harzburgite may act as a sink for high field strength elements, and probably other elements, that are present in the mantle–wedge fluids.

Communicated by J. Hoefs

V. López Sánchez-Vizcaíno (✉)
Departamento de Geología, Universidad de Jaén,
E.U. Politécnica, Alfonso X El Sabio 28,
23700 Linares, Spain
E-mail: vlopez@ujaen.es
Tel.: +34-953-648523
Fax: +34-953-648622

V. Trommsdorff · J. A. D. Connolly
Institut für Mineralogie und Petrographie,
ETH Zentrum, 8092 Zurich, Switzerland

M. T. Gómez-Pugnaire · C. J. Garrido
Departamento de Mineralogía y Petrología,
Universidad de Granada,
18002 Granada, Spain

O. Müntener
Institute of Geological Sciences,
University of Bern, 3012 Bern,
Switzerland

Introduction

Subduction of serpentinite is possibly an important process in transporting water to depths critical for the generation of arc magmas and may also account for the lower plane of double seismic zones observed in some subduction zones (e.g., Scambelluri et al. 1995; Ulmer and Trommsdorff 1995; Schmidt and Poli 1998; Kerrick 2002; Hyndman and Peacock 2003; Yamasaki and Seno 2003). In hydrated subduction zones, antigorite serpentinite may occur in large portions of the mantle wedge (Hyndman and Peacock 2003, and references therein) and the incoming subducting slab (Peacock 2001; Ranero et al. 2003; Rüpke et al. 2004). As a potentially significant dehydration reaction in subduction settings, the high-pressure breakdown of antigorite serpentinite to chlorite harzburgite (olivine + orthopyroxene + chlorite) has been investigated experimentally by several authors (Ulmer and Trommsdorff 1995; Wunder and Schreyer 1997; Bose and Navrotsky 1998;

Bromiley and Pawley 2003). Antigorite dehydration releases up to 12 wt% of H_2O making antigorite serpentinite the potentially most important source of H_2O at depths appropriate for arc magma genesis in hydrated subduction zones. Prograde chlorite harzburgite is expected to form in the mantle wedge and the slab of subduction zones (Ulmer and Trommsdorff 1995; Schmidt and Poli 1998; Hacker et al. 2003a; Rüpke et al. 2004) due to dehydration of antigorite serpentinite. There is also an increasing evidence showing that, in addition to water, serpentinite subduction products may be a suitable source and the sink of elements geochemically significant to arc volcanism such as F, Cl, B, Be, Sr and Li (Scambelluri et al. 1995, 2004a, b; Straub and Layne 2003). Garrido et al. (2005) have proposed that prograde chlorite harzburgite effectively partitions high field strength elements (HFSE = Nb, Ta, Zr and Hf), which may be a concomitant cause for HFSE depletion of arc volcanics in some subduction zones.

Many of the geochemical characteristics of high-pressure antigorite serpentinite dehydration have been accounted for the stabilization of clinohumite acting as a sink for water (McGetchin and Silver 1970), fluorine (Engi and Lindsley 1980), boron and lithium (Scambelluri et al. 2004a, b), and HFSE (Weiss and Müntener 1996; Scambelluri et al. 2001a; Garrido et al. 2005). TiCl is a member of the humite mineral suite. Humite minerals $[n(M_2SiO_4)M_{1-x}Ti_x\ (OH, F)_{2-2x}O_{2x}$, where M is Mg, Fe, Mn, Ni; n = one for norbergite, two for chondrodite, three for humite or four for clinohumite; and $X < 0.5]$ are stoichiometrically colinear with olivine, forming a polysomatic series (Thompson 1978; Veblen 1991, 1992). In contrast to a solid solution, which shows a continuous compositional variation between its endmembers, a polysomatic series consists of phases that have discrete compositions between its endmembers, namely norbergite and olivine in the case of the humite series.

Titanian clinohumite is a common accessory mineral of metamorphic ultrabasic, basic and carbonate rocks. In ultrabasic rocks, Ti-clinohumite occurs from antigorite serpentinite (Damour 1879; Brugnatelli 1904; De Quervain 1938; Bearth 1967; Möckel 1969; Trommsdorff and Evans 1980) to garnet peridotite (Möckel 1969; Evans and Trommsdorff 1983), kimberlite (McGetchin and Silver 1970), or dunite (Dymek et al. 1988). The composition and microstructural texture of TiCl, however, differ considerably from one rock type to another. For example, TiCl in antigorite serpentinite is OH- and titanium-rich, whereas, TiCl above the antigorite breakdown almost invariably contains fluorine but less titanium. These variations correspond to the three exchange vectors operating in TiCl: (1) $FeMg_{-1}$, (2) OHF_{-1} and (3) $TiO_2Mg_{-1}F_{-2}$ (Evans and Trommsdorff 1983), which have profound influence on its stability. Discontinuous breakdown of pure OH–TiCl to olivine + ilmenite + H_2O has been described and mapped to occur at a metamorphic grade below antigorite decomposition (Trommsdorff and Evans 1980). F-bearing TiCl breaks down continuously at high P and T (Evans and Trommsdorff 1983) with its F/Ti ratio increasing with grade. Experimental (Engi and Lindsley 1980; Iizuka and Nakamura 1995; Weiss 1997; Stalder and Ulmer 2001; Wirth et al. 2001) and field evidence (Yang and Jahn 2000; Trommsdorff et al. 2001; Yang 2003) indicate that TiCl is stable to pressures of at least 8 GPa (250-km depth) and temperatures well over 1,000°C.

The number of field studies with isograd mapping documenting dehydration of serpentinite rocks is rather limited (Evans and Trommsdorff 1970; Matthes 1971; Trommsdorff and Evans 1972, 1974; Springer 1974; Arai 1975; Frost 1975; Evans et al. 1976; Mellini et al. 1987; Scambelluri et al. 1995; Nozaka 2003) and, with few exceptions, they are restricted to examples of moderate pressure breakdown of antigorite to talc + olivine (< 2 GPa). A unique example of the high-pressure dehydration of antigorite serpentinite is preserved in the Cerro del Almirez ultramafic massif (Sierra Nevada, Betic Cordillera, S. Spain, Fig. 1a) (Trommsdorff et al. 1998; Hürlimann 1999; Schönbächler 1999). The general reaction forming the isograd of antigorite dehydration at Almirez is (Trommsdorff et al. 1998):

$$\begin{aligned}\text{antigorite} &\rightarrow \text{olivine} + \text{orthopyroxene} + \text{chlorite} \\ &\quad + H_2O_2(\text{serpentinite}) \\ &\rightarrow (\text{chlorite harzburgite}). \qquad (1)\end{aligned}$$

The antigorite-out isograd corresponding to this high-pressure dehydration reaction crops out in Almirez as an irregular, but as a sharp boundary separating antigorite serpentinite from chlorite harzburgite (Fig. 1b).

There are no field examples documenting the stability of Ti-clinohumite at conditions of high-pressure breakdown of antigorite serpentinite to chlorite harzburgite. At Almirez, TiCl is a common mineral in both the reactant (antigorite serpentinite) and product (chlorite harzburgite) rocks, where it occurs as OH–TiCl and F–OH–TiCl, respectively.

In this study, we investigate the textural and chemical variations of TiCl and olivine during high-pressure antigorite breakdown as recorded in the Almirez ultramafic massif. This allows us to constrain the role played by these variations in the stabilization of clinohumite and in the partitioning of HFSE into chlorite harzburgite. In addition, we estimate the P–T conditions for the equilibration of TiCl with olivine and ilmenite through thermodynamic calculations and phase diagram sections, and discuss the stability conditions of TiCl in different subduction-zone settings.

The Cerro del Almirez ultramafic massif

The most prominent lens of the ultramafic rocks within the upper sequence of the Nevado–Filábride Complex of the Betic Cordilleras occurs at the Cerro del Almirez

ultramafic massif (0.4-km thick and 2-km wide) (Fig.1). This massif is surrounded by Paleozoic sediments, where dominant pelitic rocks are interbedded with quartzite and minor marble (Hürlimann 1999; Schönbächler 1999; Gómez-Pugnaire et al. 2000). The whole sequence was metamorphosed during the Miocene under eclogite facies conditions, recording peak metamorphic conditions of ~2 GPa and ~700°C (Trommsdorff et al. 1998; Puga et al. 1999; Schönbächler 1999; López Sánchez-Vizcaíno et al. 2001).

The petrology and field occurrence of the lithologies cropping out in the Almirez ultramafic massif have been described in detail by Trommsdorff et al. (1998). The main rock types are foliated antigorite serpentinite (Atg-serpentinite) and variably textured enstatite–olivine–chlorite rocks that we will refer to as chlorite harzburgite (Chl-harzburgite). Atg-serpentinite and Chl-harzburgite are located in the northern-most and southern-most parts of the massif, respectively (Fig. 1b). Detailed field mapping shows that the boundary between the two rock types is not tectonic, but constitutes the antigorite-out isograd described above (Hürlimann 1999; Schönbächler 1999). There are also minor occurrences of metarodingite lenses and clinopyroxenite layers in scattered outcrops within both antigorite serpentinite and chlorite harzburgite.

Atg-serpentinite is strongly foliated and rather homogeneous in terms of textural and field occurrence. Chl-harzburgite, on the other hand, shows quite a variation in the textural types. The main type is spinifex-like textured Chl-harzburgite showing radiating enstatite and arborescent olivine. Granular-textured harzburgite is subordinate and formed by the deformation and recrystallization of the spinifex-like type. Synmetamorphic veins of very coarse-grained enstatite (up to 10 cm) occur close to the isograd and contain the same assemblage as Chl-harzburgite.

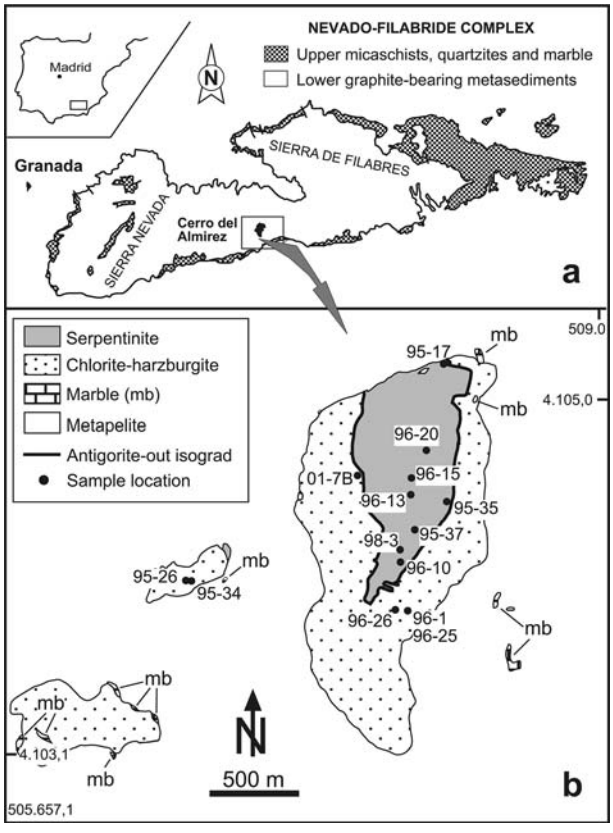

Fig. 1 **a** Outline geological map of the Nevado–Filábride Complex of the Betic Cordillera with location of the Cerro del Almirez outcrop. **b** Geological map of the Cerro del Almirez body (modified from Schönbächler 1999 and Hürlimann 1999) showing the distribution of the two main ultramafic rock types (serpentinite and chlorite harzburgite), the antigorite-out isograd and the location of the studied TiCl-bearing samples. Wall-rocks mainly consist of metapelites (*white area* surrounding ultramafic bodies) and small marble (*mb*) outcrops

Titanian clinohumite at Cerro del Almirez

In this paper, we will focus on the occurrence of TiCl in the Cerro del Almirez rocks and on its intergrowths and relationships with olivine. Several textural types of TiCl occur in antigorite serpentinite and chlorite harzburgite. Their main petrographic and chemical features are summarized in Table 1. Sample locations are shown on Fig. 1b.

Titanian clinohumite in antigorite serpentinite

In Atg-serpentinite, TiCl appears as three main textural types: as a rock-forming mineral in the serpentinite, as TiCl-rich veins near former clinopyroxenite layers, and in exsolution lamellae of clinopyroxenes (Table 1).

Rock-forming TiCl in the antigorite serpentinite occurs as a small, millimeter-sized, granoblasts, associated with dusty clinopyroxene and in many cases close to the TiCl-rich veins (see below). TiCl forms polygonal textures with antigorite, olivine and clear diopside.

The most common occurrence of TiCl in Atg-serpentinite is *within deformed veins* (2–5 cm thick). TiCl occurs together with olivine, diopside, chlorite, magnetite and ilmenite. TiCl forms up to 3 cm reddish-brown knobs together with olivine of similar size. Olivine and TiCl are locally stuffed with inclusions of needles of antigorite. Textural observations in the veins indicate that the TiCl-rich veins predate the main foliation of the rock.

The TiCl veins are locally associated with white, massive, aggregates of diopside fibres formed from former clinopyroxenite layers. TiCl-bearing pyroxenitic layers are separated from the serpentinite by a chloritic blackwall. The pyroxenites still contain large, up to 5 cm relict porphyroclasts of clinopyroxene with (100) lamellae of metamorphic diopside. Most of the former clinopyroxenite, however, consists of recrystallized folded mats and aggregates of subidiomorphic diopside, mm in size, with some chlorite. In addition, diopside

Table 1 Summary of petrographic and chemical features of titanian clinohumite (*TiCl*) from the Cerro del Almirez ultramafic massif. *P–T* conditions deduced from Fig. 9. Mineral abbreviations after Kretz (1983), except for TiCl (Evans and Trommsdorff 1983)

Rock type	TiCl type Mineral assemblage	TiCl textures	Breakdown products	Chemical variations		*P–T* conditions (TiCl + Ol + Ilm)
				TiCl	Olivine	
Atg-serpentinite	TiCl in serpentinite atg + ol + di (+ tr + chl)	Granoblastic; lamellae intergrown with olivine	Absent or very incipient	X_{Mg} = 0.89–0.92 X_F = 0–0.01 X_{Ti} = 0.42–0.47	Percentage of Fo = 90–93 Ni = 0.003–0.006 Mn = 0.005–0.007	*P* = 1.7–2.5 Gpa *T* = 620–635°C
	TiCl veins close to clinopyroxenite ol + di + chl + mgt	mm- to cm-sized knobs of TiCl and olivine	Partial or complete breakdown to olivine choked with ilmenite and magnetite inclusions	X_{Mg} = 0.89–0.92 X_F = 0–0.02 X_{Ti} = 0.42 – 0.47	Percentage of Fo = 89–92 Ni = 0.003–0.006 Mn = 0.005–0.008	
	TiCl in exsolution lamellae of dusty clinopyroxene di + chl + mgt	Strings of TiCl grains. with diopside and chlorite	Partial breakdown in the rim to ilmenite and olivine	X_{Mg} = 0.90–0.92 X_F = 0–0.006 X_{Ti} = 0.43–0.46	Not present	
Chl-harzburgite	TiCl in harzburgite ol + en + chl + mgt	Granoblastic to idiomorphic; in equilibrium with "brown" olivine and enstatite. (Fig.2a)	Partial or complete; rims with wormy ilmenite and olivine; oriented ilmenite rods. (Fig.2b)	X_{Mg} = 0.89–0.92 X_F = 0.07–0.11 X_{Ti} = 0.33–0.43	Percentage of Fo = 89–90 Ni = 0.005–0.010 Mn = 0.001–0.003	*P* = 1.7–2.07 Gpa *T* = 640–695°C
	TiCl intergrowths with "brown" olivine	Oriented lamellae or granoblastic grains intergrown with olivine (Fig.2c–f)	Partial or complete; ghost lamellae (Fig.2c–f); concentric yellow and orange zones (Fig.2f)	X_{Mg} = 0.91 – 0.92 X_F = 0.08–0.15 X_{Ti} = 0.29–0.38	Percentage of Fo = 90–91 Ni = 0.009–0.010 Mn = 0.001–0.002	
	TiCl in enstatite-rich synmetamorphic veins en + ol + chl + mgt	Xenomorphic mm-sized grains in chlorite and magnetite rich zones	Partial breakdown in the rim to ilmenite and olivine	X_{Mg} = 0.89–0.92 X_F = 0.02–0.2 X_{Ti} = 0.26–0.38	Percentage of Fo = 90Ni = 0.003–0.006 Mn = 0.001–0.004	

occurs along cracks and also as inclusions within TiCl, suggesting simultaneous crystallization of both.

In clinopyroxenites, TiCl is frequently concentrated *along former exsolution lamellae* in dusty clinopyroxene, where it forms strings of small granular or prismatic grains together with chlorite and diopside (compare Trommsdorff and Evans 1980).

The occurrence of TiCl in Atg-serpentinite and in its veins and in clinopyroxenite layers may be described by the progress of the generalized irreversible reaction

"igneous" impure clinopyroxene + olivine
+ serpentine → diopside + chlorite
+ clinohumite + H_2O (2)

(Trommsdorff and Evans 1980).

Titanian clinohumite breakdown reaction in antigorite serpentinite

In the Bergell contact aureole of the Central Alps, Trommsdorff and Evans (1980) observed breakdown of (OH)–TiCl at conditions coinciding with the isograd reaction

diopside + antigorite → tremolite
+ forsterite (+chlorite) + H_2O (3)

Both the reactant and the product assemblage of this reaction are also observed in the Atg-serpentinite of the Almirez massif. Reactants and products of the breakdown reaction of TiCl can also be observed: Almirez complete or partial breakdown of titanian clinohumite occurs according to the reaction

titanian clinohumite → olivine
+ ilmenite (+magnetite) + H_2O (4)

This reaction has only been locally observed in the foliated Atg-serpentinite but quite frequently within the TiCl veins: grains of TiCl appear partially or completely replaced by a second generation of dusty olivine, choked with a dense precipitate of tiny ilmenite granules and scarcer magnetite. Perfect optical continuity can be observed between TiCl and the new dusty olivine, as well as between the clear and the dusty olivines. This is a reflection of the previously oriented intergrowth in the clear olivine and clinohumite (Trommsdorff and Evans 1980). The transformation front between TiCl and the new olivine is very irregular: typically, small shapeless remnants of clinohumite can be found within the new olivine, and grains of olivine and ilmenite appear within the old, less transformed TiCl grains.

Ilmenite occurs as tiny *wormy grains* intergrown with olivine where the breakdown of TiCl takes place along its border, often in contact with diopside or chlorite. In contrast, the more common transformation of TiCl to a framework of olivine and *granular ilmenite and magnetite* is only observed, where clinohumite coexisted previously with clear olivine. Abrupt changes in abundance and size of the ilmenite inclusions have also been observed.

Titanian clinohumite in chlorite harzburgite

Even though it might be expected that TiCl should break down completely at the antigorite-out isograd (compare Weiss 1997), TiCl is actually present in the Almirez chlorite harzburgite in three different textural varieties: as TiCl porphyroblasts in equilibrium with olivine and enstatite, as granular and lamellar intergrowths with "brown olivine"', and as xenomorphic grains within enstatite-rich synmetamorphic veins (Table 1). As demonstrated below, TiCl in chlorite harzburgite is not a relic of pre-existing TiCl of the antigorite serpentinite.

Porphyroblastic TiCl (e.g., sample 96-1) occurs as granoblastic (≤ 2 mm), somewhat prismatic grains in zones where chlorite and magnetite are more abundant (Fig. 2a). It is optically homogeneous and is always choked with idiomorphic grains of magnetite in its core or along trails across. Porphyroblastic TiCl grains overgrow small crystals of radiating enstatite and small "brown olivine" (Trommsdorff et al. 1998). Conversely it is also found as oriented inclusion in "brown olivine". These relationships demonstrate simultaneous crystallization with "brown olivine" and enstatite in the chlorite harzburgite.

TiCl in the chlorite harzburgite invariably contains higher F (~0.4–0.6 wt% F) than OH–TiCl of the antigorite serpentinite (Table 3). Fluorine has a stabilizing effect on TiCl (Evans and Trommsdorff 1983; Weiss 1997). Because all minerals in the Atg-serpentinite, including tremolite (Trommsdorff et al. 1998, Table 1) and TiCl (Table 3), are free of fluorine, it is reasonable to assume that the bulk serpentinite is F-free. If so, F had to be introduced from fluids into the chlorite harzburgite product rocks during the crystallization of TiCl. Further evidence for this open system dehydration scenario comes from the bulk-rock trace element content of Chl-harzburgite. The strong increase of the bulk rock contents of Nb, Ta and U of Chl-harzburgite, relative to precursor Atg-serpentine requires that these trace elements were mobile and, as fluorine, were introduced by external fluids during the crystallization of Chl-harzburgite (Garrido et al. 2005). In the case of sample 96-1, the textural relationships of TiCl with other Chl-harzburgite minerals further indicate that fluid flushing likely occurred after the onset of growth of the olivine + enstatite + chlorite assemblage.

TiCl also forms part of *synmetamorphic veins* dominated by very coarse-grained enstatite crystals (up to 10 cm long). The veins contain the same assemblage as the chlorite harzburgite, with a similar amount of chlorite but much less olivine. TiCl grew in zones, rich in chlorite and opaques; it is up to 6 mm in length, and also occurs as tiny oriented inclusions in the accompanying olivine.

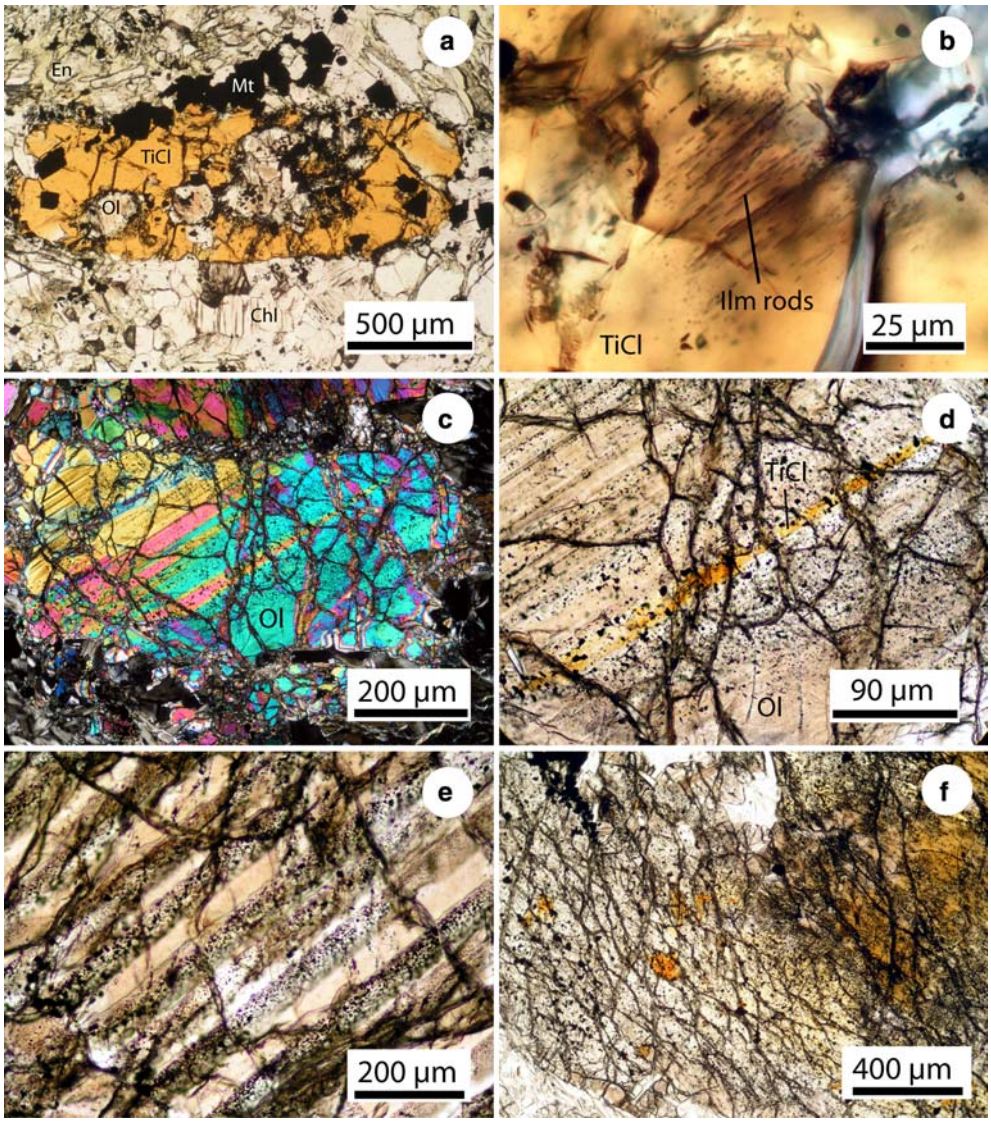

Fig. 2 **a** Prismatic F–OH–TiCl grain with inclusions of "brown olivine" in a chlorite- and magnetite-rich zone of a chlorite harzburgite rock (Sample 96-25a). **b** Oriented ilmenite rods indicating continuous breakdown reaction of F–OH–TiCl in a chlorite harzburgite (Sample 96-25b). **c** "Brown olivine" grain with intergrowths of partial or totally (ghost) broken down lamellae of F–OH–TiCl (crossed nicols) (Sample 95-34). **d** Details of the central zone of c (parallel nicols) showing a relic TiCl lamella (*orange*) and the breakdown products (granular ilmenite and clear olivine) of previous lamellae (Sample 95-34). **e** Parallel intergrowths of "brown olivine" and previous TiCl lamellae, now broken down to ilmenite and clear olivine (Sample 95-34). **f** Concentric intergrowth between "brown olivine" and granular TiCl showing orange and yellow zones, deep orange TiCl patches, and TiCl breakdown products: clear olivine and ilmenite (Sample 95-34). See text for details. Mineral abbreviations after Kretz (1983), except for TiCl (Evans and Trommsdorff 1983)

As in the case of TiCl in Atg-serpentinite, we have observed a partial or complete breakdown of TiCl in Chl-harzburgite. Most commonly, the resulting assemblage occurs in the rim of the TiCl as wormy ilmenite and olivine. In some places, oriented rods of ilmenite parallel to [001] clinohumite like those described by Trommsdorff et al. (2001) have been observed (Fig. 2b). These authors have considered these rods as typical of a continuous breakdown reaction of F–OH–TiCl. Similar features have been described by Muko et al. (2001) in garnet–TiCl–diopside rocks from the Kokchetav massif.

Intergrowths of "brown olivine" with titanian clinohumite

Oriented, lamellar intergrowths of humite minerals with olivine were first described by Tilley (1951) from the Isle of Skye. Humite–olivine intergrowths are a consequence of the similarities in structure of the two mineral suites and may occur from a nano (including polysomes) to microscopic scale (Risold 2001, her Fig. 5.5). At Almirez, microscopic intergrowths between "brown olivine" and TiCl are observed in the chlorite harzburgites (Table 1) and deserve a detailed analysis.

"Brown olivine" constitutes the main mineral of the chlorite harzburgites. It is mostly elongate and arborescent with single crystals up to 10 cm length. The core and rims of "brown olivine" are often made up of additional generations of olivine (see Trommsdorff et al. 1998). "Brown olivine" shows a weak pleochroism and contains always numerous microscopic and submicroscopic solid inclusions (Ruiz Cruz et al. 1999) among which magnetite, Cr-bearing spinel, ilmenite and other Ti-rich particles are the most common ones. Submicroscopic solid inclusions are concentrated in microscopically homogeneous domains; the microscopic-scale inclusions often occur along trails that

show various orientations. As the inclusions are oriented with respect to the olivine lattice they have been interpreted as exsolved particles (Ruiz Cruz et al. 1999). Micron-scale fluid inclusions (Scambelluri et al. 2001a; Scambelluri et al. 2004b) are common throughout the olivine generations. Domains of clear olivine within "brown olivine" occasionally contain wormy and granular ilmenite and magnetite, respectively, and we interpret them as the breakdown products of former OH–TiCl.

Titanian clinohumite occurs as overgrowth on, and as patchy inclusions within, "brown olivine". In sample 95-34, lamellar intergrowths occur with $(100)_{Ol}$ parallel to $(001)_{TiCl}$ (Fig. 2c, d). The lamellae show partial or total breakdown of TiCl (Fig. 2e). Broken down TiCl lamellae containing the typical olivine–ilmenite intergrowths are visible as ghost structures within olivine (Fig. 2c). Marginally, broken down granular TiCl displays a zonal arrangement with an orange core surrounded by a faint yellow aureole with fine-grained ilmenite and small patches of orange TiCl and by an outermost zone of "brown olivine" with ilmenite (Fig. 2f). Electron probe analyses of the orange core and the yellowish zone (Table 4: "Orange Ol" and "Yellow Ol" analyses) show SiO_2 contents similar to olivine, but it is obvious from the Ti and F contents that this zone actually constitutes a mixture of olivine with TiCl (see later). The observed "patchy" and lamellar intergrowths between olivine and TiCl in the Almirez rocks are similar to orientation relationships between these minerals reported by Wirth et al. (2001) in experimental samples.

Bulk rock composition

Selected bulk analyses of ultramafic rocks from Almirez are shown in Table 2 (see Garrido et al. 2005, Table 1, for a complete list of analyses, sample locations and analytical procedures). Atg-serpentinite and Chl-harzburgite show, with exception of CaO, good agreement in their compositions. Taking into account the much higher ignition loss of the serpentinites, the values of SiO_2, Al_2O_3, Fe_2O_3 (= Fe_{tot}), MgO and TiO_2 are in perfect agreement. CaO is significantly higher in the serpentinites, which are mostly meta-lherzolites with relict clinopyroxene, some metaclinopyroxenites and very subordinate dunitic layers (Schönbächler 1999) causing considerable variation in CaO (0.03–4.83 wt%). CaO in the chlorite harzburgites ranges from 0.06 wt% to 0.31 wt%. Ca loss of the ultramafic rocks to mafic rock types occurred at least in two stages of fluid-rich metamorphism at Almirez: in a first-stage serpentinisation and the concomitant partial breakdown of clinopyroxene was accompanied by the abundant rodingitisation of mafic dykes. In second stage, during high-pressure metamorphism, Ca-rich veins were formed at the contacts of chlorite harzburgites with wall rocks, and blackwalls were formed around mafic, rodingitic, inclusions within the chlorite harzburgite. It is inferred that Ca loss was caused by the pervasive flush of the chlorite harzburgites by the deserpentinization fluid. Thus, the lower Ca contents of the chlorite harzburgites are not necessarily in conflict with the higher Ca contents of their parental rocks, the serpentinites.

Bulk analyses of TiCl-bearing antigorite serpentinites and chlorite harzburgites are very similar to those of the TiCl absent equivalent rocks (Table 2). TiCl-rich veins occurring in the serpentinites, however, have lower MgO and higher Al_2O_3, CaO, and TiO_2 bulk contents than the serpentinites. This agrees with their origin from former clinopyroxenite layers.

In terms of trace elements, there are some marked differences between the serpentinites and the chlorite harzburgites (Garrido et al. 2005). The chlorite harz-

Table 2 Representative XRF bulk analyses of the Cerro del Almirez ultramafic rocks

Rock type	Antigorite serpentinite			Average (nine samples)	σ	Chlorite harzburgite		Average (13 samples)	σ	Antigorite serpentinite with TiCl		Chlorite harzburgite with TiCl	TiCl vein in antigorite serpentinite
Sample	95-17	95-35	98-3			95-34	95-26			90-1	96-15A		
SiO_2	40.19	41.78	40.08	40.54	0.69	45.58	40.79	42.76	1.44	40.91	39.29	42.72	39.74
Al_2O_3	2.40	3.35	2.70	2.75	0.46	2.65	1.65	2.52	0.72	2.69	3.51	1.61	5.71
Fe_2O_3	7.42	7.30	8.51	8.06	0.45	7.87	8.28	8.31	0.37	8.63	9.95	8.11	6.09
MnO	0.11	0.10	0.10	0.11	0.02	0.11	0.12	0.12	0.02	0.13	0.09	0.12	0.13
MgO	37.29	33.98	37.70	36.35	1.71	40.07	42.57	40.72	1.36	34.45	35.43	42.68	30.90
CaO	2.28	4.83	0.03	2.45	1.88	0.09	0.18	0.12	0.07	5.07	2.01	0.07	9.04
Na_2O	bdl	bdl	bdl			0.00	bdl	0.00	0.00	bdl	0.00	0.00	0.00
K_2O	bdl	bdl	bdl			0.00	bdl	0.00	0.00	bdl	0.00	0.00	0.00
TiO_2	0.05	0.11	0.12	0.17	0.21	0.07	0.11	0.08	0.04	0.10	0.21	0.02	1.50
P_2O_5	0.01	0.01	0.02	0.02	0.01	0.05	0.04	0.03	0.03	0.01	0.01	0.02	0.77
Zr (ppm)	8.9	6.00	7.40	13.70	16.28	9.90	78.90	15.77	21.75	7.1	8.10	5.50	189.30
LOI	10.37	8.96	11.62	10.07	1.15	3.70	4.62	5.01	1.70	8.05	10.32	5.15	6.39
Total	100.12	100.42	100.88	100.51	0.44	100.20	98.36	99.66	0.88	100.04	100.82	100.49	100.27

LOI loss on ignition; *bdl* below detection limit

burgites show statistically much higher Nb/La, Ta/La, Zr/Sm and Hf/Sm ratios than precursor serpentinites. They show gains of Nb, Ta and U relative to serpentinite. For a detailed account see Garrido et al. (2005).

Compositional variations of titanian clinohumite, olivine and their intergrowths

Analytical methods

Tables 3 and 4 show compositional variations of TiCl and coexisting olivine in all lithologies. The compositional features of other minerals in these lithologies are described in detail in Trommsdorff et al. (1998). Minerals have been analysed at the Universidad de Granada with an electron microprobe Cameca SX50 equipped with four wavelength-dispersive spectrometers. As natural and synthetic standards were used: natural fluorite (F), natural sanidine (K), synthetic $MnTiO_3$ (Ti, Mn), natural diopside (Ca), synthetic Fe_2O_3 (Fe), natural albite (Na), natural periclase (Mg), synthetic SiO_2 (Si), synthetic Cr_2O_3 (Cr), synthetic NiO (Ni), natural willemite (Zn), and synthetic Al_2O_3 (Al). An accelerating voltage of 20 kV, with a beam current of 30 nA and a beam diameter of ~2 mm were used to analyze opaque minerals. The analytical conditions for silicates were: 20 kV, 20 nA and a beam diameter of ~5–6 mm. Counting times on peak were twice those of background, with 15 s for Na and K; 20 s for F, Ti and Ca; 25 s for Fe, Si, Al, Mn, Zn and Ni; and 30 s for Mg and Cr. The crystal configuration of the microprobe was PCO crystal (F), PET crystal (K, Ti, Ca, Cr), LiF crystal (Fe, Mn, Ni, Zn), and TAP crystal (Na, Mg, Si, Al). The Na and K were always counted first (simultaneously) to avoid alkali loss. No appreciable decrease in counting statistics were expected for Na and K during their counting times (15 s), according to the experiments carried out by García Casco et al. (1993). The detection limits for F, Ni and Zn were 0.09, 0.09 and 0.08%, respectively. The data were reduced using the procedure of Pouchou and Pichoir (1985).

Element-distribution X-ray (XR) maps of the minerals were obtained with the CAMECA SX-50 operated at 20 kV and 200 nA. The XR intensities were measured at step sizes and counting times of 3 μm and 200 ms, respectively. The images were processed using Adobe Photoshop software.

Table 3 Representative analyses of TiCl from different rocks and textural positions

Textural type	TiCl in antigorite serpentinite		TiCl vein in antigorite serpentinite		TiCl in cpx lamella	TiCl in chlorite harzburgite		TiCl intergrowth with ""brown olivine"		TiCl in enstatite-rich vein	
Sample	96-20	96-20	96-15B	96-15B	96-10	96-1C	96-1C	95-34	95-34	01-7B	01-7B
SiO_2	36.88	36.65	36.51	36.64	36.55	36.34	36.01	36.93	36.02	35.95	36.85
TiO_2	5.53	5.42	5.38	5.57	5.61	5.08	4.89	3.89	4.50	4.34	3.27
Cr_20_3	0.01	0.01	0.02	0.00	0.01	0.05	0.14	0.07	0.01	0.02	0.00
Al_20_3	0.00	0.00	0.00	0.00	0.00	0.00	0.00	0.00	0.00	0.00	0.00
FeO	6.77	7.22	8.82	7.45	7.55	8.21	7.72	8.30	7.64	8.75	7.63
MgO	48.56	48.34	47.14	48.05	47.69	48.31	49.11	49.10	48.64	46.97	49.63
MnO	0.36	0.31	0.31	0.36	0.40	0.14	0.11	0.14	0.11	0.10	0.17
NiO	0.12	0.18	0.17	0.14	0.17	0.24	0.23	0.31	0.24	0.18	0.13
CaO	0.02	0.02	0.00	0.00	0.01	0.01	0.00	0.01	0.00	0.01	0.01
Na_20	0.03	0.02	0.01	0.01	0.01	0.00	0.00	0.00	0.00	0.00	0.01
K_2O	0.01	0.01	0.01	0.01	0.01	0.00	0.01	0.00	0.00	0.01	0.00
F	0.00	0.00	0.02	0.03	0.00	0.43	0.62	0.48	0.72	0.52	1.12
Total	98.25	98.17	98.38	98.26	98.01	98.81	98.84	99.23	97.88	96.85	98.82
O = F	0.00	0.00	0.01	0.01	0.00	0.18	0.26	0.20	0.30	0.22	0.47
Total	98.26	98.18	98.37	98.24	98.01	98.63	98.59	99.03	97.58	96.63	98.35
Ions calculated on the basis of 13 cations											
Si	4.010	3.994	4.001	3.999	4.003	3.957	3.910	3.987	3.949	4.001	3.994
Ti	0.452	0.444	0.444	0.457	0.462	0.416	0.399	0.316	0.371	0.363	0.267
Cr	0.000	0.000	0.001	0.000	0.000	0.002	0.006	0.003	0.000	0.000	0.000
Al	0.000	0.000	0.000	0.000	0.001	0.000	0.000	0.000	0.000	0.001	0.000
Fe^{2+}	0.616	0.658	0.808	0.680	0.692	0.748	0.701	0.749	0.701	0.814	0.692
Mg	7.870	7.851	7.699	7.815	7.785	7.840	7.946	7.901	7.947	7.791	8.017
Mn	0.033	0.029	0.028	0.033	0.037	0.013	0.010	0.013	0.010	0.009	0.016
Ni	0.010	0.015	0.015	0.012	0.015	0.021	0.020	0.027	0.021	0.016	0.011
Ca	0.002	0.002	0.000	0.000	0.001	0.001	0.000	0.001	0.000	0.001	0.001
Na	0.003	0.002	0.001	0.001	0.001	0.000	0.000	0.000	0.000	0.000	0.001
K	0.000	0.001	0.001	0.000	0.001	0.000	0.001	0.000	0.000	0.001	0.000
F	0.000	0.000	0.006	0.010	0.000	0.148	0.213	0.164	0.250	0.183	0.384
X_{Mg}	0.927	0.923	0.905	0.920	0.918	0.913	0.919	0.909	0.916	0.905	0.921
X_F	0.000	0.000	0.003	0.005	0.000	0.074	0.106	0.082	0.125	0.092	0.192
X_{Ti}	0.452	0.444	0.444	0.457	0.462	0.416	0.399	0.316	0.371	0.363	0.267

Table 4 Representative analyses of olivine from different rocks and textural positions

Textural type	Ol in antigorite serpentinite	Ol in TiCl vein	"Brown Ol" in chlorite harzburgite	Ol in enstatite-rich vein	Llamellar intergrowth of TiCl and "brown olivine"						Concentric intergrowth of TiCl and "brown olivine"			
					Clear Ol	Homogeneous "brown Ol"	Orange lamella	"Brown Ol" close to lamella	Clear Ol close to lamella	"Ghost" lamella	Clear Ol	"Brown Ol" from border	"Orange Ol"	"Yellow Ol"
Sample	96-20	96-15B	96-1C	01-7B	95-34 (1)	95-34 (1)	95-34 (1)	95-34 (1)	95-34 (1)	95-34 (1)	95-34 (2)	95-34 (2)	95-34 (2)	95-34 (2)
SiO_2	40.58	41.27	40.75	40.60	40.20	39.93	38.69	40.10	39.71	39.97	40.28	39.53	39.05	39.48
TiO_2	0.00	0.03	0.00	0.01	0.00	0.02	2.13	0.19	0.06	0.09	0.02	0.13	1.24	0.60
Cr_2O_3	0.01	0.01	0.01	0.00	0.00	0.17	0.04	0.01	0.01	0.08	0.00	0.07	0.17	0.04
Al_2O_3	0.00	0.00	0.00	0.00	0.00	0.00	0.00	0.00	0.00	0.00	0.00	0.00	0.00	0.00
FeO	7.68	7.39	8.41	9.16	8.87	9.09	8.59	8.30	8.78	9.00	8.53	8.88	8.82	8.88
MgO	50.63	50.51	50.35	49.01	50.24	49.72	49.82	50.85	50.53	50.40	50.56	49.79	49.62	50.28
MnO	0.33	0.32	0.09	0.14	0.11	0.10	0.11	0.12	0.14	0.10	0.11	0.09	0.11	0.08
NiO	0.22	0.29	0.35	0.21	0.46	0.52	0.39	0.38	0.52	0.45	0.48	0.47	0.42	0.40
CaO	0.01	0.00	0.00	0.01	0.01	0.00	0.00	0.01	0.00	0.00	0.00	0.01	0.01	0.00
Na_2O	0.00	0.01	0.02	0.01	0.00	0.00	0.00	0.00	0.01	0.00	0.00	0.00	0.00	0.01
K_2O	0.01	0.01	0.01	0.00	0.00	0.01	0.01	0.00	0.00	0.00	0.01	0.01	0.00	0.00
F	0.04	0.00	0.02	0.06	0.01	0.02	0.17	0.05	0.00	0.00	0.02	0.00	0.10	0.16
Total	99.51	99.83	100.01	99.21	99.90	99.58	99.95	100.01	99.76	100.09	100.01	98.98	99.54	99.93
0 = F	0.02	0.00	0.01	0.03	0.00	0.01	0.07	0.02	0.00	0.00	0.01	0.00	0.04	0.07
Ions calculated on the basis of three cations														
Total	99.49	99.83	100.00	99.19	99.90	99.57	99.88	99.99	99.76	100.09	100.00	98.98	99.50	99.86
Si	0.993	1.003	0.994	1.001	0.981	0.980	0.950	0.975	0.969	0.973	0.980	0.974	0.961	0.965
Al	0.000	0.000	0.000	0.000	0.000	0.000	0.000	0.000	0.000	0.000	0.000	0.000	0.000	0.000
Ti	0.000	0.001	0.000	0.000	0.000	0.000	0.039	0.003	0.001	0.002	0.000	0.002	0.023	0.011
Cr	0.000	0.000	0.000	0.000	0.000	0.002	0.000	0.000	0.000	0.001	0.000	0.001	0.002	0.000
Fe^{2+}	0.157	0.150	0.172	0.189	0.181	0.186	0.176	0.169	0.179	0.183	0.174	0.183	0.182	0.182
Mn	0.007	0.007	0.002	0.003	0.002	0.002	0.002	0.002	0.003	0.002	0.002	0.002	0.002	0.002
Mg	1.846	1.830	1.831	1.802	1.827	1.818	1.823	1.842	1.837	1.829	1.834	1.828	1.820	1.832
Ni	0.004	0.006	0.007	0.004	0.009	0.010	0.008	0.007	0.010	0.009	0.009	0.009	0.008	0.008
Ca	0.000	0.000	0.000	0.000	0.000	0.000	0.000	0.000	0.000	0.000	0.000	0.000	0.000	0.000
Na	0.000	0.000	0.001	0.000	0.000	0.000	0.000	0.000	0.000	0.000	0.000	0.000	0.000	0.000
K	0.000	0.000	0.000	0.000	0.000	0.000	0.000	0.000	0.000	0.000	0.000	0.000	0.000	0.000
X_{Fo}	0.922	0.924	0.914	0.905	0.910	0.907	0.912	0.916	0.911	0.909	0.914	0.909	0.909	0.910

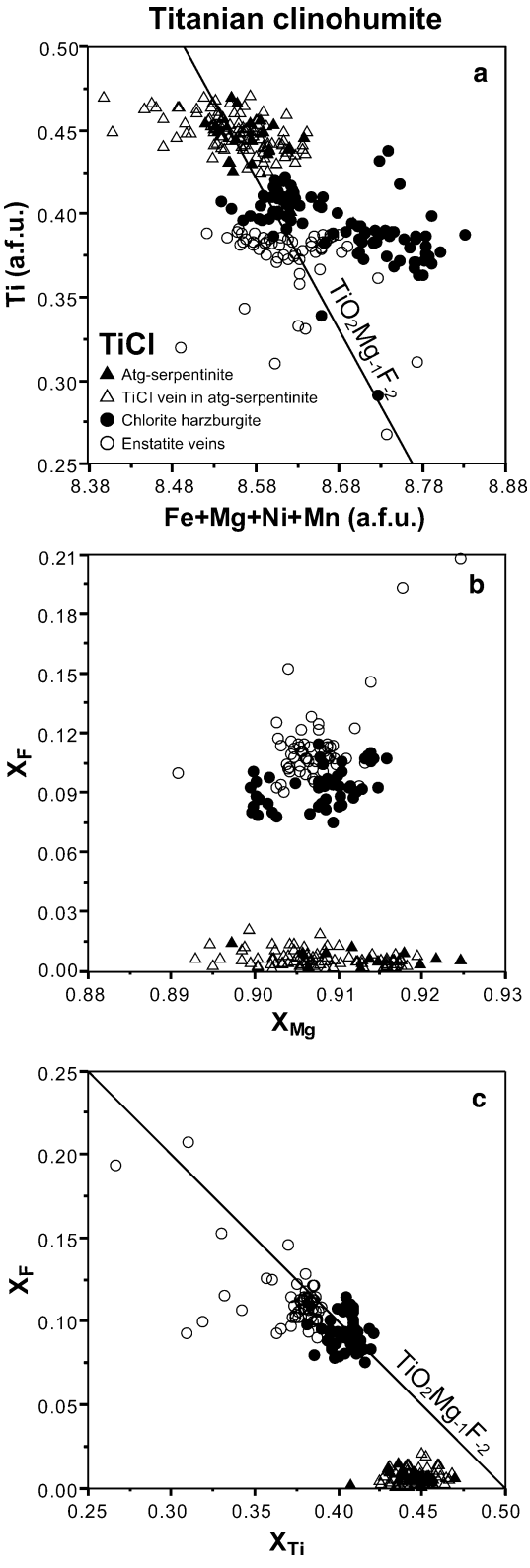

◀

Fig. 3 Compositional features of titanian clinohumite (TiCl) from different occurrences in the Almirez outcrop. **a** Ti versus Fe + Mg + Ni + Mn, **b** X_F versus $X_{Mgtotal}$; and **c** X_F versus X_{Ti} for all TiCl. TiCl in exsolution lamellae of clinopyroxene (not shown for the shake of clarity) matches the chemical variation of TiCl in serpentinite. *Continuous trendlines* (**a** and **c**) display the theoretical compositional variation of vector $TiO_2Mg_{-1}F_{-2}$ as defined by Evans and Trommsdorff (1983). $X_{Mg} = Mg/(Mg + Fe + Mn + Ni)$; $X_F = F/2$; $X_{Ti} = Ti$

Mineral trace element data for Fig. 8 were obtained in sample thick sections by Laser Ablation-ICP-MS (LA-ICP-MS) at The Open University (UK) using a frequency quintupled Nd:YAG UV (213 nm) laser system (UP213, Merchanteck-New Wave Research) linked to an HP7500a ICP-MS. Analytical procedures, as well as details on the accuracy and reproducibility of the analyses, are reported elsewhere (Garrido et al. 2005).

Titanian clinohumite

Microprobe analyses of TiCl (Table 3) from occurrences on both sides of the antigorite-out isograd show variations along the exchange vectors $FeMg_{-1}$, OHF_{-1}, and $TiO_2Mg_{-1}F_{-2}$ (Evans and Trommsdorff 1983). This variation is recognized between the different types of TiCl occurrence, but no obvious compositional zoning was observed within individual TiCl grains. In a Ti versus Fe + Mg + Ni + Mn atoms per formula unit (afu) plot (Fig. 3a), TiCl analyses follow a trend which is consistent with 1:1 exchange of cations along the vector $TiO_2Mg_{-1}F_{-2}$.

TiCl in Atg-serpentinite is F-free, but shows a narrow variation along the vector $FeMg_{-1}$ from $X_{Mg} = 0.891$ to $X_{Mg} = 0.925$ (Fig. 3b), which is controlled by the bulk-rock composition. The clinohumites of the Atg-serpentinites are close to the maximum saturation in Ti ($X_{Ti} = 0.5$, based on the crystal-chemical considerations, see Ribbe 1979) at values of about $X_{Ti} = 0.42$–0.47 (Fig. 3c). This is in agreement with their lack of fluorine. TiCl of chlorite harzburgites contains 0.43–1.2 wt % of fluorine, which translates into X_F of 0.07–0.20 (Fig. 3b, c). The presence of fluorine stabilizes TiCl at the prevailing metamorphic conditions. The variation of $FeMg_{-1}$ in the Chl-harzburgite TiCl ($X_{Mg} = 0.90$ to $X_{Mg} = 0.92$) is even narrower than in the serpentinites, which could be interpreted as homogenization due to the pervasive presence of fluid during deserpentinization. In a X_F versus X_{Ti} plot, all TiCl analyses are aligned, almost ideally, along the exchange vector $TiO_2Mg_{-1}F_{-2}$ (Fig. 3c). Variation in this trend is introduced by the uncertainty due to the possible presence of Fe^{3+}. This is specially marked in some TiCl analyses from the enstatite-rich veins (open circles on Fig. 3c).

Figure 3c displays a nice grouping of the analytical data of TiCl with the highest titanium and no fluorine in the serpentinites; with fluorine contents of < 0.1 X_F ($X_F = F/F + OH$) in the chlorite harzburgite and somewhat higher values in the enstatite-rich veins within chlorite harzburgite. These data suggest an introduction of fluorine into the chlorite harzburgite from an external reservoir together with a fluid of some elevated SiO_2 content, but still buffered by the coexistence of orthopyroxene and olivine.

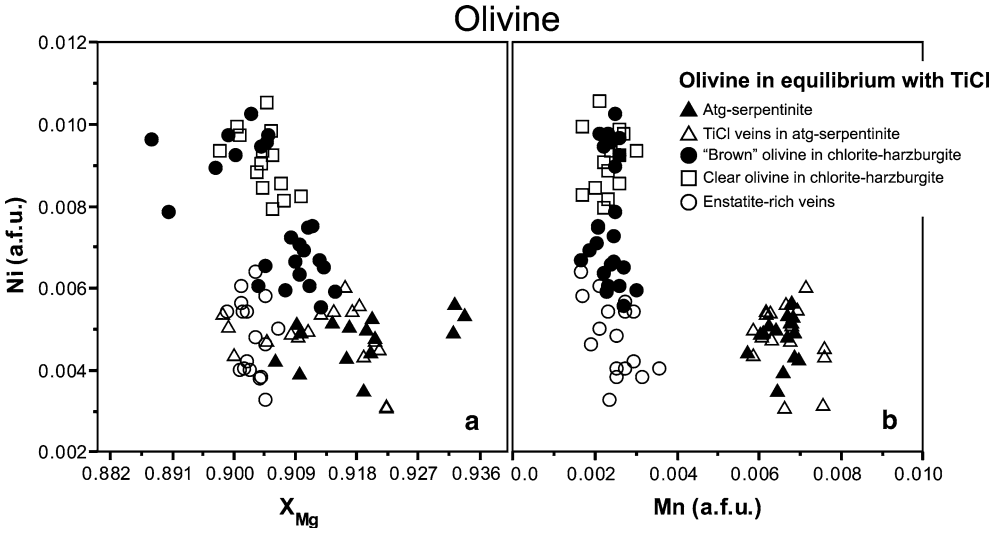

Fig. 4 Compositional features of olivine in equilibrium with titanian clinohumite from different occurrences in the Almirez outcrop. **a** Ni (a.f.u.) versus $X_{Mgtotal}$; and **b** Ni (a.f.u.) versus Mn (a.f.u.)

Olivine

Olivine shows some compositional variation according to its occurrence in different rock types. Forsterite (Fo) contents (Fig. 4a) vary from 89% in "brown olivine" from chlorite harzburgite to over 93% in olivine from antigorite serpentinite and in olivine formed by the breakdown of TiCl. The greatest variation of Fo content is observed in the serpentinites and in veins, whereas the variation is distinctly smaller in the chlorite harzburgites. In general, the olivines follow the well- known trend of Ni versus Mg as established in meta-ultramafic rocks (Trommsdorff and Evans 1974; Frost 1975). Ni in olivine (Fig. 4a, b) varies over a factor of three among antigorite serpentinite, enstatite-rich veins and the chlorite harzburgite. A grouping into enstatite-free and enstatite-bearing rocks is obvious in terms of the Mn content in olivine (Fig. 4b: Ni vs Mn): olivine from serpentinite and veins has 0.006–0.008 afu Mn, whereas, olivine from the chlorite harzburgite contains ~0.002 afu Mn. The low values of Mn in the Chl-harzburgite olivine are due to preferential partitioning of Mn into enstatite (Trommsdorff et al. 1998). The partitioning of divalent cations between olivine and TiCl (Table 5) is nearly equal for Mn and Mg, except for TiCl veins in Atg-serpentinite, where Mg concentrates preferentially in olivine (Fig. 5a, b). Olivine also shows a preference for Ni and TiCl for Fe, although there is a lot of scatter for the latter (Fig. 5a, c). The corresponding partition coefficients for TiCl with the other minerals are also shown in Table 5.

Microscopic, concentric and lamellar, *oriented intergrowths between olivine and TiCl* have been analysed in Chl-harzburgite sample 95-34 (Table 4). From core to rim of the concentric intergrowth, zones are observed that grade in colour from orange through yellow to nearly colourless into a rim of "brown olivine". The zones show increasing precipitation of ilmenite towards the rim, but the outermost zone of "brown olivine" is almost free of microscopic ilmenite inclusions (Fig. 2f). Small, orange patches of TiCl occur in all the zones. Chemical analyses of these zones, taking F and TiO_2 as indicators, fall off a mixing line between olivine (margin) and TiCl (patches) of the zoned intergrowth (Fig. 6a). Similar relationships hold for the lamellar intergrowths of both minerals (Fig. 6b). "Brown olivines" plot somewhat off the origin of the diagrams with most of the analyses sharing the trend given by the yellow and orange zones (Fig. 6a) or the orange lamellae (Fig. 6b). This trend intersects the line of the compositional variation of F–OH–TiCl at 4.7% TiO_2 (Fig. 6a). This means that the TiCl patches (Fig. 6a) and the microscopic TiCl lamellae (Fig. 6b) have continued to exchange F and TiO_2 along the vector $TiO_2Mg_{-1}F_{-2}$ after the mixing trend had been established.

The zoned intergrowth is interpreted as a continuous breakdown of TiCl with olivine plus ilmenite growing (reaction 4) at its expense. Similar relationships may be derived from a lamellar intergrowth in the same sample, where TiCl lamellae share extinction positions with ghost lamellae of clear olivine within "brown olivine" (Fig. 2c). We also observed trails of wormy ilmenite along lamellae of olivine within "brown olivine" (Fig. 2e). These lamellae are interpreted as ghost structures of former TiCl.

This interpretation is supported by the X-ray maps showing the distribution of F, Ti, and Fe (Fig. 7) in the same olivine grain as in Fig. 2c, d. XR images also illustrate the negative correlation between F and Ti in these lamellar intergrowths during continuous prograde breakdown of F–OH–TiCl. The strong preferential partitioning of fluorine into TiCl explains the concentration of all the available F in the remaining TiCl lamellae (green patches in Fig. 7a) and the increasing F/Ti ratios in this mineral with metamorphic grade (Evans and Trommsdorff 1983; Weiss 1997; Scambelluri et al. 2001b; Garrido et al. 2005). Accordingly, the remaining TiCl grains (oriented red lamellae in Fig. 7b) cannot

hold all Ti present in the system. Ti concentrates in the breakdown products of previous TiCl: microscopic sized granular ilmenites (scattered red points in Fig. 7b), and Ti-rich submicroscopic inclusions (green lamellae and zones in Fig. 7b).

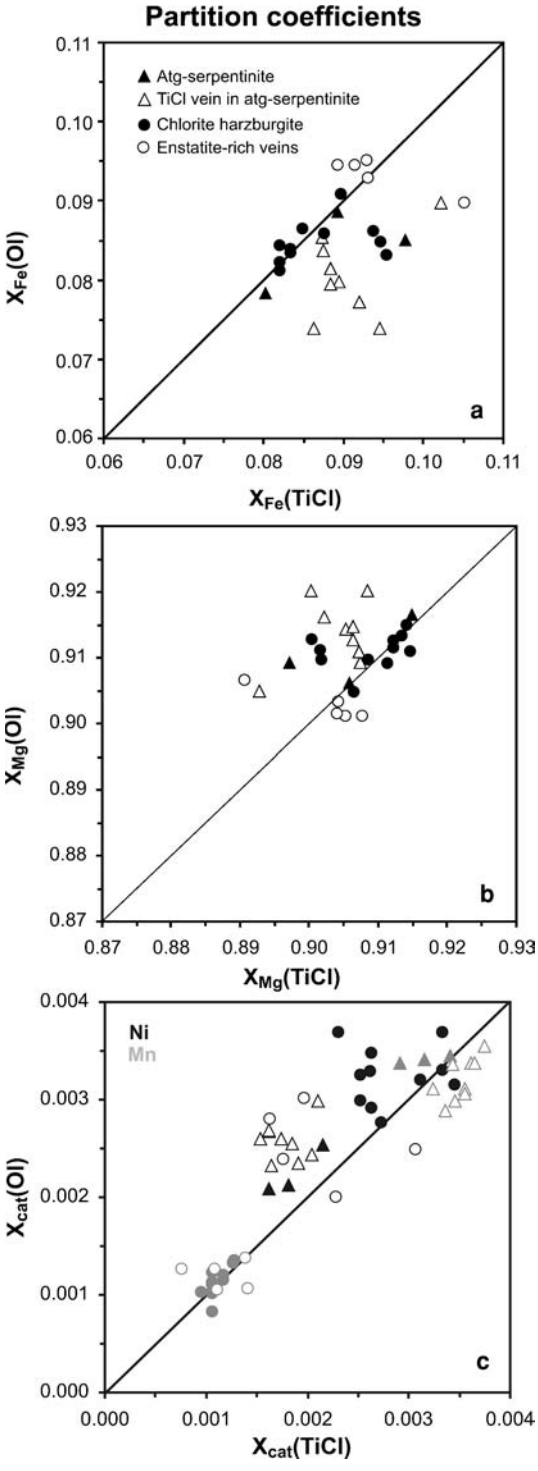

Fig. 5 Partitioning of Fe **(a)**, Mg **(b)**, and Ni and Mn **(c)** between TiCl and olivine in the reported occurrences. See Table 5 for KD's

The *concentration of HFSE* in the different textural types of olivine (Fig. 8) provides further evidence for the presence of TiCl intergrowths and/or their breakdown products within Chl-harzburgite olivines. Titanian clinohumite is a well-known reservoir of HFSE in peridotitic rocks (Weiss 1997; Scambelluri et al. 2001b; Garrido et al. 2005). In good agreement with the previous work, our LA-ICP-MS analyses of TiCl in different Almirez rock types confirm that this phase concentrates on Nb, Ta, and to a lesser extent, Zr and Hf (Fig. 8a, b). The content of Nb and Ta of clear olivine in Almirez Chl-harzburgite is, on the other hand, orders of magnitude lower than that of TiCl from Almirez and elsewhere (Fig. 8a), but similar to that of mantle olivines in orogenic peridotites and mantle xenoliths (Sun and Kerrich 1995; Bedini and Bodinier 1999; Garrido et al. 2000). When the concentrations of HFSE with like ionic radius and charge are plotted against each other (i.e., Hf vs Zr and Ta vs Nb), there is a positive correlation of the concentrations of HFSE in olivines belonging to different textural types, with clear olivines displaying the lowest contents of HFSE, and "brown" and "yellow" olivines showing increasingly higher contents of these elements. Titanian clinohumites plot at high contents of HFSE in these plots (Fig. 8).

P–T conditions

Calculation methods

We estimate the *P–T* conditions at which OH–TiCl and F–OH–TiCl were stable in Atg-serpentinite and Chl-harzburgite, respectively. Phase diagram sections (pseudosections) were calculated for bulk-rock compositions from the Almirez and the results compared with the observed phase relationships in the rocks. Reliable thermodynamic data for TiCl are lacking in any of the available thermodynamic databases. Thus, to estimate the conditions of equilibration for the TiCl, we derived properties for the endmember $Mg_7^{M0}(Mg_{1.5}Ti_{0.5})^{M3}Si_4O_{16}\left(O_{3/4}(OH)_{1/4}\right)_{4/3}^{O3}(OH)_{2/3}^{O2}$ based on the structure refinements of Robinson et al. (1973), where M0 designates all octahedral sites other than M3, O3 designates the two hydroxyl sites about M3; and O2 designates the single hydroxyl site associated with the M2,5 octahedral site. Assuming an ideal mixing, the activity of the TiCl endmember is $a_{ticl} = \frac{256}{3^{2/3}}\left(z_{Mg}^{M0}\right)^7\left(z_{Mg}^{M3}z_{Ti}^{M3}\right)^2\left(z_{O}^{O3}z_{OH}^{O3}\right)^{4/3}\left(z_{OH}^{O2}\right)^{2/3}$, where z_j^i is the molar site fraction of species j on site i. The vibrational and volumetric components of the TiCl equation of state were computed as a stoichiometrically weighted linear combination of the properties of forsterite, geikielite, and rutile as reported by Holland and Powell (1998, revised 2002). The standard state Gibbs energy of formation from the elements $G_{ticl}^{o} = -9104.019$ kJ/mol and third-law entropy

Table 5 Partition coefficients (K_D) for Fe, Mg, Ni and Mn between olivine and other minerals and coexisting TiCl

Min/TiCl	K_DFe	K_DMg	K_DNi	K_DMn
Ol in antigorite serpentinite	0.938	1.059	1.213	1.084
Ol in TiCl veins	0.880	1.127	1.462	0.913
"Brown Ol" in chlorite harzburgite	0.972	1.026	1.163	1.009
Ol in enstatite-rich veins	0.996	1.006	1.261	1.096
Atg in antigorite serpentinite	0.738	1.401	0.173	0.542
Chl in TiCl veins	0.586	1.760		0.105
Chl in Cpx lamellae	0.662	1.590	1.095	0.108
Chl in Chlorite harzburgite	0.509	1.930	1.065	0.178
Chl in enstatite-rich veins	0.583	1.702	1.024	0.196
Chl average	0.585	1.745	1.059	0.147
Cpx in antigorite serpentinite	0.460	2.019	1.628	0.840
Cpx in TiCl veins	0.348	2.796	0.247	0.843
En in Chlorite harzburgite	1.002	1.015	0.267	1.582
En in enstatite-rich veins	1.098	0.926	0.380	1.963
Tr in Chlorite harzburgite	0.549	1.923	0.576	0.267

$K_D = (X_{cat}(min)\times 1\text{-}X_{cat}(TiCl))/(1\text{-}X_{cat}(min)\times X_{cat}(TiCl))$

Table 6 Phase notation and thermodynamic data sources. Unless indicated otherwise, thermodynamic data was taken from Holland and Powell (1998, revised 2002). The compositional variables x and y may vary between zero and unity and are determined as a function of pressure and temperature by free-energy minimization (Connolly 2005, in press). Thermodynamic data for the iron end-members for antigorite and brucite were estimated as described in Rüpke et al. (2004).

Symbol	Phase	Formula	Source
Ath	Anthophyllite	$Mg_{7x}Fe_{7(1-x)}Si_8O_{22}(OH)_2$	Ideal
Atg	Antigorite	$Mg_{48x}Fe_{48(1-x)}Si_{34}O_{85}(OH)_{62}$	(Rüpke et al. 2004)
Chlorite	Chlorite	$Mg_{(5-y+z)x}Fe_{(5-y+z)\ (1-x)}Al_{2(1+y-z)}Si_{3-y+z}O_{10}(OH)_8$	(Holland et al. 1998)
Cpx	Clinopyroxene	$CaMg_xFe_{(1-x)}Si_2O_6$	(Holland and Powell 1996)
Ol	Olivine	$Mg_{2x}Fe_{2(1-x)}SiO_4$	(Holland and Powell 1998)
Opx	Orthopyroxene	$Mg_{x(2-y)}Fe_{(1-x)(2-y)}Al_{2y}Si_{2-y}O_6$	(Holland and Powell 1996)
Tlc	Talc	$Mg_{(3-y)x}Fe_{(3-y)(1-x)}Al_{2y}Si_{4-y}O_{10}(OH)_2$	(Holland and Powell 1998)
Tr	Clinoamphibole	$Ca_2Mg_{(3+2y)x}Fe_{(3+2y)(1-x)}Al_{3-3y}Si_{7+y}O_{22}(OH)_2$	(Wei and Powell 2003; White et al.2003)

$S^o_{ticl} = 389.8825$ J/mol for TiCl were obtained by fitting the conditions for the decomposition of TiCl to ilmenite, olivine and water at 0.5 GPa and 823 K (runs mw32/37–47), and at 2.0 GPa and 983 K (runs mw35–37) established experimentally by Weiss (1997). To this end, endmember activities for TiCl in clinohumite, geikielite in ilmenite and forsterite in olivine were computed from the observed mineral compositions for ideal ionic mixing models

($\{a_{ticl} = 0.299,\ a_{geik} = 0.331,\ a_{fo} = 0.800\}$ at 823 K and $\{a_{ticl} = 0.304,\ a_{geik} = 0.372,\ a_{fo} = 0.922\}$ at 983 K), and the fluid phase was assumed to be pure water with properties given by the CORK equation of state (Holland and Powell 1998).

The conditions for the equilibration of TiCl with ilmenite and olivine (reaction 4) in the serpentinites of interest here (thick dashed curve in Fig. 9) were estimated from the thermodynamic data as described above for the mineral compositions observed in the serpentinite sample 96-15b ($\{a_{ticl} = 0.409,\ a_{geik} = 0.319, a_{fo} = 0.878\}$).

These conditions compare reasonably well with the phase diagram sections computed for Ca-poor (sample 95-17, Fig. 9a, b) and Ca-rich (sample 95-35, Fig. 9c, d) serpentinite bulk compositions from the Almirez (Table 2). In these diagrams (calculated for the system SiO_2–Al_2O_3–MgO–FeO–CaO), the mineral assemblages corresponding to those observed in the serpentinites (antigorite + olivine + chlorite + tremolite) shift their stability fields towards higher temperature conditions for increasing bulk X_{Mg} values ($X_{Mg} = MgO/(MgO + FeO)$). Although bulk-iron contents (Table 2) are expressed as total Fe_2O_3, in the serpentinites, the only important Fe_2O_3-bearing phase is magnetite. Thus, all Fe_2O_3 present in magnetite was removed for the calculations and the remaining total Fe_2O_3 converted to FeO. Modal amounts of magnetite may reach up to 10% in the Almirez serpentinites (Schönbächler 1999). For each type of bulk composition, several diagrams were computed for different amounts of magnetite with the typical composition of this mineral reported by Trommsdorff et al. (1998, Table 1).

Results

For the Ca-poor serpentinite, the phase diagram section with 5 wt% magnetite (Fig. 9a) better fits the observed

phase relationships in these rocks. The absence of talc and the presence of tremolite in the prograde paragenetic sequence imply a maximum temperature of 635°C and pressures in the range of 1.7–2.05 GPa for the stability of the serpentinite. For this pressure range, the temperature of the clinohumite + olivine + ilmenite equilibrium is 620–635°C, consistent with the observation that clinohumite decomposes within the stability field of Atg-serpentinites. For higher magnetite amounts (Fig. 9b), the OH–TiCl + olivine + ilmenite equilibrium (4) takes place within the stability field of tremolite-free serpentinites.

In Ca-richer bulk serpentinite compositions, phase relationships similar to those of Fig. 9a are only obtained for a phase diagram section with 7 wt% magnetite and, hence, higher X_{Mg} ratios (Fig. 9d). Observed tremolite–antigorite-bearing serpentinite is stable to a maximum temperature of 640°C and pressures in the range of 1.7–2.07 GPa. For these conditions, TiCl breakdown takes place at temperatures ranging from 620°C to 635°C within the stability field of the Atg-serpentinites. In agreement with our partitioning data (Table 5), at lower X_{Mg} ratios (magnetite below 6 wt%, Fig. 9c), the computed phase diagram sections show completely different phase relationships. Talc-bearing assemblages and chlorite harzburgites with tremolite do not develop at any *P–T* conditions. This gives an idea of how much the uncertainty in bulk composition affects the topology of phase diagram sections and suggests that the presence or absence of talc is very sensitive to X_{Mg} and CaO and, therefore, the absence of this mineral is not necessarily an indication of high pressure.

Pressure–temperature conditions for the F-bearing TiCl cannot be estimated with precision since consistent

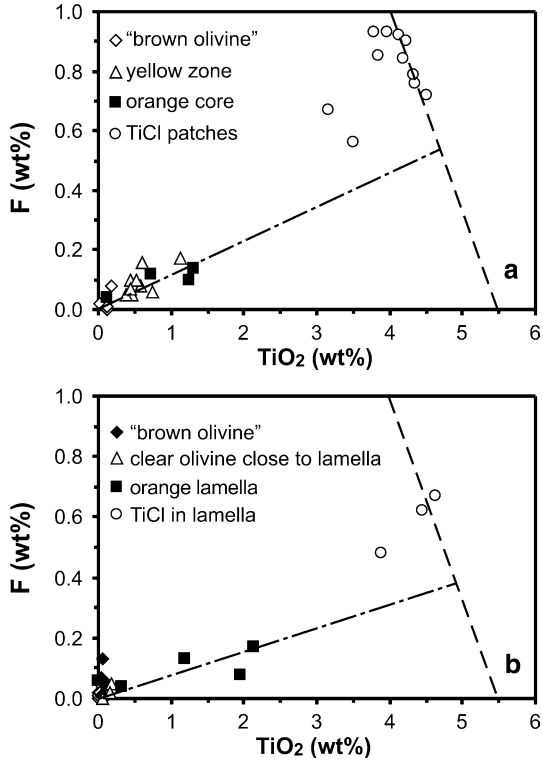

Fig. 6 Variation of TiO_2 and F contents in TiCl and olivine in concentric **(a)** and lamellar **(b)** intergrowths shown in Fig. 2f, c and d, respectively. *Dashed lines* show the observed compositional variation of TiCl. Strong scatter of two points in (**a**) and one point in (**b**) owes most probably to analytical inaccuracy produced by small-scale intergrowths with olivine. *Dashed-dotted lines* show the theoretical mixing trend between olivine and TiCl. *Intersection of the two lines* gives the original composition of the TiCl endmember of the mixing trend

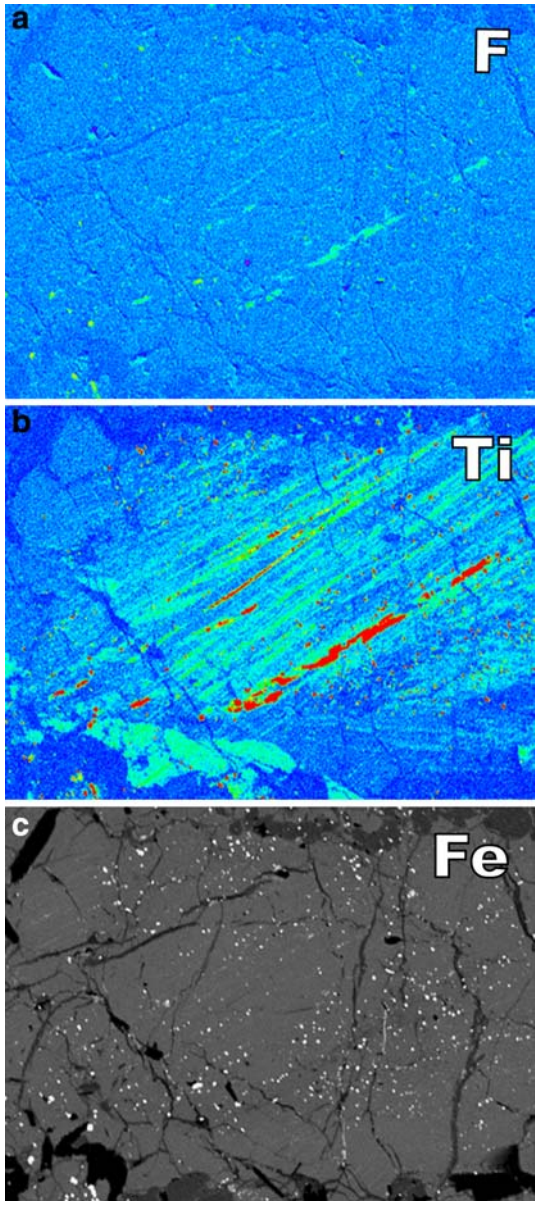

Fig. 7 XR images showing the distribution of F, Ti, and Fe in oriented lamellar intergrowths of TiCl in "brown olivine" (same grain as in Fig. 2c, d). Note the different behaviour of F and Ti after the breakdown of TiCl. In the first case (**a**), all F concentrates in the remaining TiCl lamellae (*green patches*); in the case of Ti (**b**), it occurs in the form of TiCl (*red*), but also with an homogeneous distribution within brown olivine (*green zones*). In **c**, bright areas denote higher Fe concentration

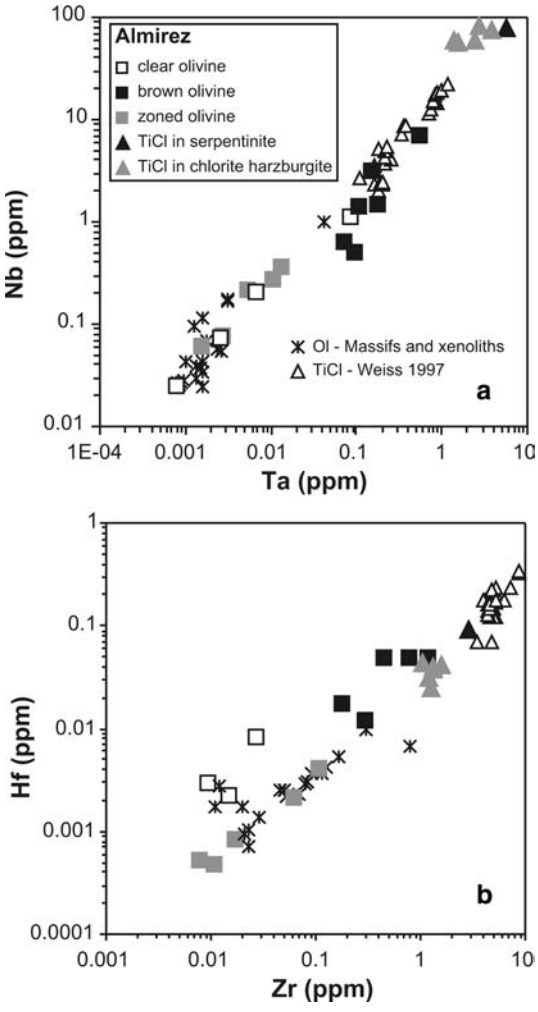

Fig. 8 Plot of the content of Nb versus Ta (**a**) and Hf versus Zr (**b**) in different textural types of olivine and TiCl in the Almirez ultramafic massif. Also shown in the figure are LA-ICP-MS analyses of TiCl in ultramafic rocks from different Alps localities (Weiss 1997), and LA-ICP-MS and bulk analyses of olivine in peridotites from ultramafic massifs and xenoliths (Bedini and Bodinier 1999; Garrido et al. 2000; Sun and Kerrich 1995). Note as there is a steady increase in these HFSE from clear olivine to brown olivine, which has HFSE contents close to those of F–OH–TiCl from Almirez and elsewhere. This is interpreted as additional evidence for precursor TiCl intergrowths in brown olivine

thermodynamic data calculations are not feasible. Textural relationships in the chlorite harzburgites, nevertheless, clearly indicate the simultaneous growth of TiCl with spinifex-like olivine and orthopyroxene. According to Fig. 9a and d this would have happened at temperatures above 640°C in a pressure range of 1.7–2.07 GPa (dotted area). The estimated *P*–*T* path for the Almirez ultramafic massif shows that the temperature peak was reached in these rocks close to peak pressure conditions and was followed by a sharp cooling and decompression (López Sánchez-Vizcaíno et al. 2001). Thus, the maximum temperatures reached by the Chl-harzburgites are those constrained by the higher temperature stability field of the assemblage chlorite + clinopyroxene + orthopyroxene + olivine, an assemblage that is not present at the Almirez ultramafics, in a range from 640°C to 695°C (Fig. 9a, d).

Discussion and conclusions

Metamorphic evolution of TiCl-bearing rocks

In both of the two ultramafic rock types at Cerro del Almirez, the earlier antigorite serpentinite and the later chlorite harzburgite, a characteristic generation of TiCl has been recognised. Compositional and textural features discussed here indicate that the total breakdown of OH–TiCl occurred beyond the antigorite-out isograd. New formation of F–OH–TiCl in equilibrium with "brown olivine" and enstatite took place in the presence of some fluorine, due to fluid infiltration after the onset of dehydration.

TiCl in Atg-serpentinites is saturated in Ti (X_{Ti} ≈0.46) and F-free, whereas in TiCl of Chl-harzburgite, about 10 mol% of the total Ti is substituted by the fluorine along the exchange vector $TiO_2Mg_{-1}F_{-2}$ (X_{Ti} ≈0.41, X_F ≈0.1). The overall variation in the composition of each of the generations is small and extends only over a few mol% along the vectors $FeMg_{-1}$, $TiO_2Mg_{-1}F_{-2}$ and OHF_{-1} (Fig. 3). The relative homogeneity of TiCl and its consistent element partitioning with coexisting minerals (Table 5) in both rock types is taken as an indication that each system closely attained equilibrium during metamorphism. Complete or partial breakdown of OH–TiCl has been observed in veins within antigorite serpentinite and locally in the serpentinite. Pseudomorphs of clear olivine with ilmenite after TiCl also occur as inclusions within olivine of the chlorite harzburgite, which otherwise is dominated by F–OH–TiCl with quite constant X_F ≈0.1. These data are taken as evidence that, for OH–TiCl and in the absence of fluorine, the equilibrium (4) was slightly surpassed. In the chlorite harzburgite, with some fluorine present, the equilibrium was closely approached for the F–OH–TiCl of this rock. The curve for breakdown of the given OH–TiCl in the antigorite serpentinites is superposed on the *P*–*T* phase diagram section of Fig. 9a, d. This isopleth may be compared with the assemblages of the phase diagram section fields corresponding to those observed in the Almirez ultramafic rocks: at $P = 1.7$–2.05 GPa it matches the stability conditions for the fields Chl–Cpx–Tr–Ol–Atg or Chl–Tr–Ol–Atg. These assemblages occur in the Almirez serpentinites. Textural relationships indicate simultaneous growth of F–OH–TiCl and the chlorite harzburgite paragenesis, corresponding to the field Chl–Opx–Tr–Ol of Fig. 9. We therefore assume that the climax of metamorphism in the antigorite serpentinite was about 630°C and in the chlorite harzburgite 20°C higher. This climax is similar in pressure, but somewhat higher in temperature than the conditions derived by Schönbächler (1999) for kyanite–garnet–

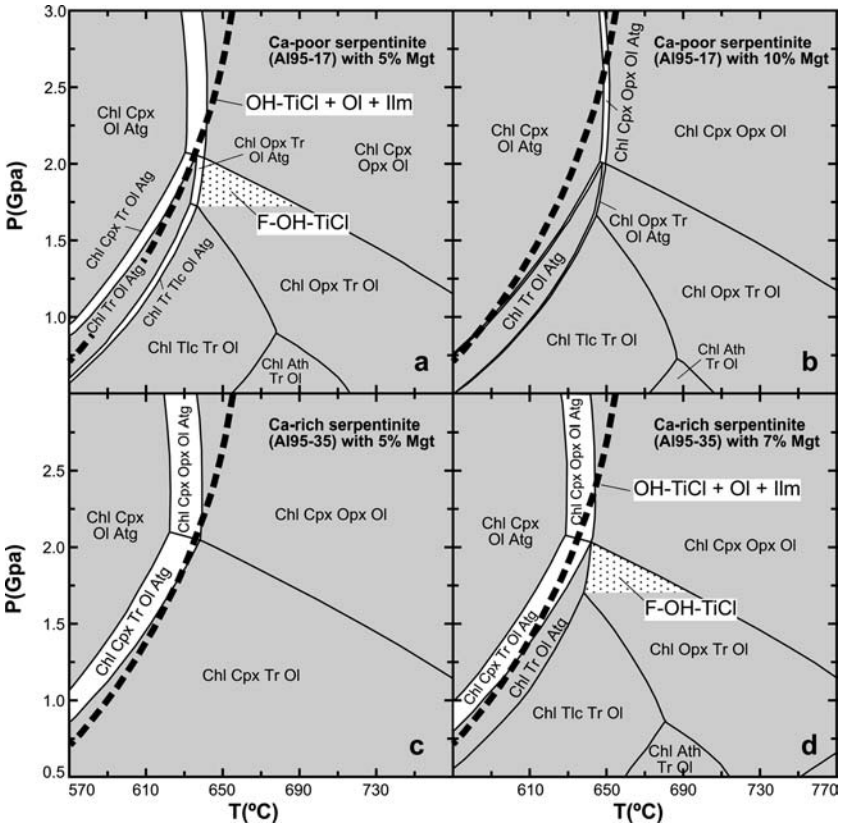

Fig. 9 Pressure–temperature phase diagram sections (system SiO_2–Al_2O_3–MgO–FeO–CaO) computed with Perplex (Connolly 2005, in press) for typical Ca-poor (sample 95-17, **a** and **b**) and Ca-rich (sample 95-35, **c** and **d**) serpentinite bulk compositions and different amounts of magnetite (see text for details). Estimated pressure–temperature conditions for the OH–TiCl + Ol + Ilm equilibrium (*thick dashed curve*) in the serpentinite sample 96-15B were computed with Perplex using data as described in the text and superposed on the diagram. Estimated *P*–*T* conditions (*dotted areas*) for the stability of F–OH–TiCl from the chlorite harzburgites of the Almirez are only shown in those diagrams (**a** and **d**), which better reproduce the observed field relationships in the studied rocks. See Table 6 for phase notation and data sources

quartz–graphite–chloritoid rocks of the area (~600°C, ~2 GPa).

Fluid infiltration

Mapping of mineral assemblages within the Almirez ultramafic rocks (Hürlimann 1999; Schönbächler 1999) provided evidence for an antigorite-out isograd (Fig. 1) according to reaction (1). This isograd cuts across an otherwise continuous ultramafic body. It is evident from the field relationships that the two ultramafic rock types at Almirez shared this metamorphism. However, with respect to their H_2O budget during metamorphism, considerable differences between serpentinite and chlorite harzburgite are evident. Whereas, the unreacted antigorite serpentinite mostly retained its bulk H_2O content (~10 wt% H_2O) during metamorphism (Table 1), the product chlorite harzburgite contains only an average of 5 wt% H_2O (fixed in chlorite). This means that during metamorphism, the chlorite harzburgite must have been flushed by H_2O liberated from the deserpentinization reaction. As a consequence, the spinifex-like texture of the assemblage of "brown olivine", enstatite, chlorite, and TiCl is formed. This assemblage acted as a sink for HFSE ("brown olivine" and TiCl) (Garrido et al. 2005), for Cl (chlorite), Li (TiCl), and B (olivine and TiCl) (Scambelluri et al. 2004b), and for F (TiCl; in the serpentinite all minerals are F-free). These elements, perhaps with the exception of Cl and B (Scambelluri et al. 2004b), are enriched relative to the serpentinite (Garrido et al. 2005). At the same time Ca was lost from the chlorite harzburgite assemblage to mafic layers and to country rocks.

The bulk enrichment of HFSE, Li and F within the chlorite harzburgite strongly suggests an addition of external, crustal fluid to the reacting ultramafic rocks (Garrido et al. 2005). Infiltration of external fluid into the chlorite harzburgite rocks is also supported by the occurrence of enstatite-rich veins, which have a drastically higher SiO_2 (~55 wt%) content than the hosting chlorite harzburgite (~42 wt% SiO_2). For comparison, the average SiO_2 content of the serpentinites is about 40 wt%. As antigorite is a very sluggish reactant (Evans et al. 1976; Trommsdorff 1983; Evans 2004), it must be considered that the onset of deserpentinization at Almirez was triggered by the introduction of an external fluid.

Origin and significance of "brown olivine"

In view of the importance of TiCl as a sink for HFSE, TiCl has been considered as a potential candidate causing the well-known HFSE depletion of arc magmatism (Weiss and Müntener 1996; Weiss 1997; Garrido et al. 2005). Its petrographic occurrence and relationship with "brown olivine" at Almirez therefore deserves special attention.

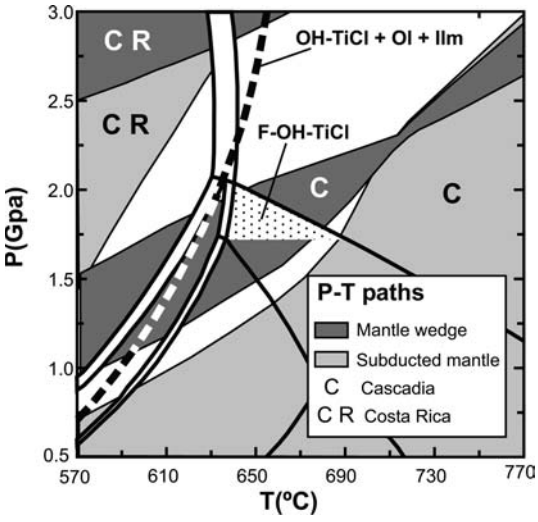

Fig. 10 Pressure–temperature phase diagram section (corresponding to that from Fig. 9a) comparing the estimated *P–T* conditions for the OH–TiCl and F–OH–TiCl from the Almirez with the *P–T* paths calculated by Hacker et al. (2003a) for the subducted mantle and the mantle wedge just above the subducting crust in the Cascadia and Costa Rica subduction zones.

Given the low quantities of optically recognizable TiCl within the chlorite harzburgites (overall $<<0.1\%$, but in individual samples up to 10%), it is worthwhile considering the budget and mode of Ti and HFSE storage within these rocks. Besides TiCl (10^2 of Nb and Ta when normalized to the primitive upper mantle of Sun and McDonough 1989), the most important candidate for Ti, Nb and Ta storage is "brown olivine" (Garrido et al. 2005, Fig. 3 and Table 2). "Brown olivine" consistently accommodates about 1.5 orders of magnitude less of these elements than TiCl, but forming over 50 vol% of the rock, "brown olivine" is at least two to three orders of magnitude more abundant than TiCl. "Brown olivine" is therefore considered the main carrier of Ti, Nb and Ta (144, 1.3, and 0.082 ppm, respectively, Garrido et al. 2005).

From electron microscopy studies, it is known that in HP peridotites, the quantity of planar, polysomatic, humite-type defects parallel to (001) olivine can reach a volume of up to $10^{-1.5}$% (Sykes et al. 1994; Risold et al. 2001; compilation in Drury 1991; Risold 2001). If these planar defects were Ti-saturated TiCl, this would correspond to over 200 ppm Ti (Risold 2001). Already reacted planar defects increase the possible Ti amounts in olivine up to 350 ppm, as determined by independent spectroscopic (Reusser et al. 1998) and EMPA methods (Hacker et al. 1997). Thus, all the Ti observed in "brown olivine" at Almirez (144 ppm, after LA-ICP-MS analyses in Garrido et al. 2005) and the correlated HFSE, Nb and Ta (see above), could easily be stored in planar (001) humite-type defects. However, the TEM study of Ruiz Cruz et al. (1999) of "brown olivine" showed only exsolved oxide particles and, among those, numerous micro-platelets of ilmenite. Pre-existing (001) defects would then have to be annealed out and Ti and HFSE stored in the exsolved ilmenite.

The existence of microscopic, interlayered TiCl–olivine structures parallel to (001) in "brown olivine" has, however, been demonstrated in this paper. The existence of olivine + ilmenite ghost lamellae in these parallel intergrowths demonstrates that even some microscopic TiCl lamellae within "brown olivine" have been annealed out at Almirez. In our opinion, it is therefore reasonable to assume that Ti, Nb and Ta were stored along planar (001) humite defects and in intergrowths within "brown olivine" (see also Fig. 7).

Once chlorite harzburgites are formed and Ti and HFSE are stored in the rock, the storage is maintained even if the TiCl and its intergrowths break down. Ti and HFSE then are stored in the product ilmenite that highly partitions HFSE (Bodinier et al. 1996; Ionov et al. 1999; Kalfoun et al. 2002).

Stability of titanian clinohumite in subduction zones

Despite their subordinate abundance in ultramafic rocks, humite group minerals have been demonstrated to be of considerable interest for the understanding of processes taking place in the hydrated subduction zones. Titanian clinohumite, in particular, acts as a sink for water, F, B, Li, and HFSE, and is stable at depths at which significant dehydration reactions occur, which account for the generation of arc magmatism and double seismic zones in subduction settings. The potential stability of TiCl with different compositions in subduction environments has been shown by Weiss (1997, her Fig. 6.28). In hydrated, intermediate to warm subduction zones TiCl–olivine intergrowths, similar to those studied here, can be stable in prograde chlorite harzburgite at pertinent sub-arc depths both in the subducting slab mantle and the wedge of mantle above the slab. This can be shown (Garrido et al. 2005, Fig. 6) after mapping of relevant deserpentinization (Ulmer and Trommsdorff 1995; Wunder and Schreyer 1997) and clinohumite breakdown reactions (Weiss 1997; Trommsdorff et al. 2001), and the use of conventional thermal models (e.g. Hacker et al. 2003a; Yamasaki and Seno 2003) for subduction zones.

The mantle wedge has been proposed as a feasible environment for the formation of the TiCl-bearing chlorite harzburgites of the Almirez ultramafic complex (Garrido et al. 2005). We can come to similar conclusions if we compare the deduced stability conditions for the Almirez TiCl with the *P–T* paths deduced by Hacker et al. (2003a) for both the slab mantle (clear shading) and the mantle wedge just above the slab (dark shading) in subduction zones with different thermal regimes (Fig. 10). There is a good match between the *P–T* conditions determined for the studied TiCl, at both sides of the deserpentinization reaction (thick dashed curve for OH–TiCl and dotted area for F–OH–TiCl, respectively), and the *P–T* conditions calculated for the mantle wedge

(just above the slab) in the Cascadia subduction zone (Fig. 10). In this kind of a warm subduction zone (Hacker et al. 2003b), the stability of TiCl at equivalent or higher pressures in the slab mantle would only occur at significantly higher temperatures. At these conditions, TiCl should be richer in fluorine (Evans and Trommsdorff 1983). In colder subduction zones like Costa Rica, TiCl would be stable only at pressures and temperatures above 3 GPa and 670°C, respectively (Fig. 10).

The TiCl–olivine intergrowths in chlorite harzburgites reported in this work formed at maximum depths of 65 km (2 GPa), well above the depths at which dehydration melting takes place in most subduction zones. Despite this and other uncertainties, the Almirez ultramafic complex is the only known natural example in which reactants and products of the antigorite-out isograd, together with two generations of TiCl, crop out and can be mapped in the field. Accordingly, this complex must be considered as a significant proxy for deserpentinization reactions and their implications for the understanding of subduction environments.

Acknowledgements We wish to thank B.W. Evans and B. Wunder for their review on this manuscript. This work is supported by the Spanish "Ministerio de Educación y Ciencia" through research grant BTE 2004-1489 and a "Ramón y Cajal" fellowship (CJG) and the "Junta de Andalucía" research groups RNM-0145 and RNM-0131. We thank Olivier Alard (The Open University) for LA-ICP-MS analyses.

References

Arai S (1975) Contact metamorphosed dunite–harzburgite complex in Chugoku District, Western Japan. Contrib Mineral Petrol 52:1–16

Bearth P (1967) Die Ophiolithe der Zone von Zermatt-Saas Fee. Beitr Geol Karte Schweiz NF 132:130

Bedini RM, Bodinier JL (1999) Distribution of incompatible trace elements between the constituents of spinel peridotite xenoliths: ICP-MS data from the East African Rift. Geochim Cosmochim Acta 63:3883–3900

Bodinier JL, Merlet C, Bedini RM, Simien F, Remaidi M, Garrido CJ (1996) Distribution of niobium, tantalum, and other highly incompatible trace elements in the lithospheric mantle: the spinel paradox. Geochim Cosmochim Acta 60:545–550

Bose K, Navrotsky A (1998) Thermochemistry and phase equilibria of hydrous phases in the system $MgO–SiO_2–H_2O$: implications for volatile transport to the mantle. J Geophys Res-Solid Earth 103:9713–9719

Bromiley GD, Pawley AR (2003) The stability of antigorite in the systems $MgO–SiO_2–H_2O$ (MSH) and $MgO–Al_2O_3–SiO_2–H_2O$ (MASH): the effects of Al^{3+} substitution on high-pressure stability. Am Miner 88:99–108

Brugnatelli L (1904) Über den Titanolivin der Umgebung von Chiesa in Val Malenco; ein Beitrag zur Kenntnis des Titanolivin. Z Kristallogr Miner 39:209–219

Connolly JAD (2005) Computation of phase equilibria by linear programming: a tool for geodynamic modeling and its application to subduction zone decarbonation. Earth Planet Sci Lett (in review)

Damour M (1879) Note sur le peridot titanifère de Zermatt en Valais. Bull Soc Fr Miner 2:15

De Quervain T (1938) Zur Kenntnis des Titanklinohumites (Titanolivine). Schweiz Mineral Petrogr Mitt 18:591–604

Drury MR (1991) Hydration-induced climb dissociation of dislocations in naturally deformed mantle olivine. Phys Chem Miner 18:106–116

Dymek RF, Boak JL, Brothers SC (1988) Titanian chondrodite-bearing and titanian clinohumite-bearing metadunite from the 3,800 Ma Isua Supracrustal Belt, West Greenland—Chemistry, Petrology, and Origin. Am Miner 73:547–558

Engi M, Lindsley DH (1980) Stability of titanian clinohumite—experiments and thermodynamic analysis. Contrib Mineral Petrol 72:415–424

Evans BW (2004) The serpentinite multisystem revisited: chrysotile is metastable. Int Geol Rev 46:479–506

Evans BW, Johannes W, Oterdoom H, Trommsdorff V (1976) Stability of chrysotile and antigorite in the serpentinite multisystem. Schweiz Miner Petrogr Mitt 56:79–93

Evans BW, Trommsdorff V (1970) Regional metamorphism of ultramafic rocks in the Central Alps: parageneses in the system $CaO–MgO–SiO_2–H_2O$. Schweiz Miner Petrogr Mitt 50:481–492

Evans BW, Trommsdorff V (1983) Fluorine-hydroxyl titanian clinohumite in Alpine recrystallized garnet peridotite: compositional controls and petrologic significance. Am J Sci 283:355–369

Frost BR (1975) Contact metamorphism of serpentinite, chloritic blackwall and rodingite at Paddy-Go-Easy Pass, Central Cascades, Washington. J Petrol 16:272–313

García Casco A, Sánchez Navas A, Torres Roldán RL (1993) Disequilibrium decomposition and breakdown of muscovite in high P–T gneisses, Betic Alpine Belt (Southern Spain). Am Miner 78:158–177

Garrido CJ, Bodinier JL, Alard O (2000) Incompatible trace element partitioning and residence in anhydrous spinel peridotites and websterites from the Ronda orogenic peridotite. Earth Planet Sci Lett 181:341–358

Garrido CJ, López Sánchez-Vizcaíno V, Gómez-Pugnaire MT, Trommsdorff V, Alard O, Bodinier JL, Godard M (2005) Enrichment of HFSE in chlorite–harzburgite produced by high-pressure dehydration of antigorite–serpentinite: implications for subduction magmatism. Geochem Geophys Geosyst 6:Q01J15. doi:10.1029/2004GC000791

Gómez-Pugnaire MT, Braga JC, Martín JM, Sassi FP, Del Moro A (2000) Regional implications of a Palaeozoic age for the Nevado–Filabride Cover of the Betic Cordillera, Spain. Schweiz Miner Petrogr Mitt 80:45–52

Hacker BR, Abers GA, Peacock SM (2003a) Subduction factory—1. Theoretical mineralogy, densities, seismic wave speeds, and H_2O contents. J Geophys Res Solid Earth 108:art. no. 2029

Hacker BR, Peacock SM, Abers GA, Holloway SD (2003b) Subduction factory —2. Are intermediate-depth earthquakes in subducting slabs linked to metamorphic dehydration reactions? J Geophys Res Solid Earth 108:art. no. 2030

Hacker BR, Sharp T, Zhang RY, Liou JG, Hervig RL (1997) Determining the origin of ultrahigh-pressure lherzolites. Science 278:702–704

Holland TJB, Baker J, Powell R (1998) Mixing properties and activity-composition relationships of chlorites in the system $MgO–FeO–Al_2O_3–SiO_2–H_2O$. Eur J Miner 10:395–406

Holland TJB, Powell R (1996) Thermodynamics of order–disorder in minerals.2. Symmetric formalism applied to solid solutions. Am Miner 81:1425–1437

Holland TJB, Powell R (1998) An internally consistent thermodynamic data set for phases of petrological interest. J Metamorph Geol 16:309–343

Hürlimann R (1999) Die Hochdruckmetamorphose der Ultramafika und der angrenzenden Nebengesteine am Cerro de Almirez, Sierra Nevada, Südspanien. Teil II. Unpublished Diplomarbeit. ETH, Zürich, pp 105

Hyndman RD, Peacock SM (2003) Serpentinization of the forearc mantle. Earth Planet Sci Lett 212:417–432

Iizuka Y, Nakamura E (1995) Experimental study of the slab-mantle interaction and implications for the formation of titanoclinohumite at deep subduction zone. Proc Jpn Acad Ser B-Phys Biol Sci 71:159–164

Ionov DA, Gregoire M, Prikhod'ko VS (1999) Feldspar-Ti-oxide metasomatism in off-cratonic continental and oceanic upper mantle. Earth Planet Sci Lett 165:37–44

Kalfoun F, Merlet C, Ionov D (2002) Determination of Nb, Ta, Zr and Hf in micro-phases at low concentrations by EPMA. Mikrochim Acta 139:83–91

Kerrick D (2002) Serpentinite seduction. Science 298:1344–1345

Kretz R (1983) Symbols for rock-forming minerals. Am Miner 68:277–279

López Sánchez-Vizcaíno V, Rubatto D, Gómez-Pugnaire MT, Trommsdorff V, Müntener O (2001) Middle Miocene high-pressure metamorphism and fast exhumation of the Nevado–Filabride Complex, SE Spain. Terra Nova 13:327–332

Matthes S (1971) Die ultramafischen Hornfelse, inbesondere ihre Phasenpetrologie. Fortschritte Der Mineral 48:109–127

McGetchin TR, Silver LT (1970) Compositional relations in minerals from kimberlite and related rocks in the Moses Rock dike, San Juan County, Utah. Am Miner 55:1738–1771

Mellini M, Trommsdorff V, Compagnoni R (1987) Antigorite polysomatism— behavior during progressive metamorphism. Contrib Mineral Petrol 97:147–155

Möckel JR (1969) Structural petrology of the garnet peridotite of Alpe Arami (Ticino), Switzerland. Leidse Geol Meded 42:61–130

Muko A, Yoshioka N, Ogasawara Y, Zhu Y, Liou J (2001) Petrography and mineral chemistry of TiCl-bearing garnet rock from Kokchetav ultra high-pressure belt. In: UHPM workshop. Waseda University, pp 190–193

Nozaka T (2003) Compositional heterogeneity of olivine in thermally metamorphosed serpentinite from Southwest Japan. Am Miner 88:1377–1384

Peacock SM (2001) Are the lower planes of double seismic zones caused by serpentine dehydration in subducting oceanic mantle? Geology 29:299–302

Pouchou JL, Pichoir F (1985) PAP $\phi(\rho z)$ procedure for improved quantitative microanalysis. In: Armstrong JT (ed) Microbeam analysis. San Francisco Press Inc., San Francisco, pp 104–106

Puga E, Nieto JM, Díaz de Federico A, Bodinier JL, Morten L (1999) Petrology and metamorphic evolution of ultramafic rocks and dolerite dykes of the Betic Ophiolitic Association (Mulhacen Complex, SE Spain): evidence of eo-Alpine subduction following an ocean-floor metasomatic process. Lithos 49:23–56

Ranero CR, Morgan JP, McIntosh K, Reichert C (2003) Bending-related faulting and mantle serpentinization at the Middle America trench. Nature 425:367–373

Reusser E, Risold AC, Günther D, Trommsdorff V (1998) Bulk Ti-content of ilmenite-bearing olivine from garnet lherzolites. EOS Trans AGU 79: F953

Ribbe PH (1979) Titanium, fluorine, and hydroxyl in the humite minerals. Am Miner 64:1027–1035

Risold AC (2001) Formation of oxide inclusions in olivine from garnet peridotites (Central Alps). Phd Thesis. ETH, Zürich, pp 111

Risold AC, Trommsdorff V, Grobety B (2001) Genesis of ilmenite rods and palisades along humite-type defects in olivine from Alpe Arami. Contrib Miner Petrol 140:619–628

Robinson K, Gibbs GV, Ribbe PH (1973) Crystal-structures of humite minerals. 4. Clinohumite and titanoclinohumite. Am Miner 58:43–49

Ruiz Cruz MD, Puga E, Nieto JM (1999) Silicate and oxide exsolution in pseudo-spinifex olivine from metaultramafic rocks of the Betic Ophiolitic Association: a TEM study. Am Miner 84:1915–1924

Rüpke LH, Morgan JP, Hort M, Connolly JAD (2004) Serpentine and the subduction zone water cycle. Earth Planet Sci Lett 223:17–34

Scambelluri M, Bottazzi P, Trommsdorff V, Vannucci R, Hermann J, Gómez-Pugnaire MT, López Sánchez-Vizcaíno V (2001a) Incompatible element-rich fluids released by antigorite breakdown in deeply subducted mantle. Earth Planet Sci Lett 192:457–470

Scambelluri M, Fiebig J, Malaspina N, Müntener O, Pettke T (2004a) Serpentinite subduction: implications for fluid processes and trace-element recycling. Int Geol Rev 46:595–613

Scambelluri M, Müntener O, Hermann J, Piccardo GB, Trommsdorff V (1995) Subduction of water into the mantle—history of an Alpine Peridotite. Geology 23:459–462

Scambelluri M, Müntener O, Ottolini L, Pettke T, Vannucci R (2004b) The fate of B, Cl and Li in the subducted oceanic mantle and in the antigorite breakdown fluids. Earth Planet Sci Lett 222:217–234

Scambelluri M, Rampone E, Piccardo GB (2001b) Fluid and element cycling in subducted serpentinite: a trace-element study of the Erro–Tobbio high-pressure ultramafites (Western alps, NW Italy). J Petrol 42:55–67

Schmidt MW, Poli S (1998) Experimentally based water budgets for dehydrating slabs and consequences for arc magma generation. Earth Planet Sci Lett 163:361–379

Schönbächler M (1999) Die Hochdruckmetamorphose der Ultramafika und der angrenzenden Nebengesteine am Cerro de Almirez, Sierra Nevada, Südspanien. Teil I. Unpublished Diplomarbeit. ETH, Zürich, pp 113

Springer RK (1974) Contact metamorphosed ultramafic rocks in Western Sierra–Nevada Foothills, California. J Petrol 15:160–195

Stalder R, Ulmer P (2001) Phase relations of a serpentine composition between 5 and 14 GPa: significance of clinohumite and phase E as water carriers into the transition zone. Contrib Mineral Petrol 140:670–679

Straub SM, Layne GD (2003) The systematics of chlorine, fluorine, and water in Izu arc front volcanic rocks: implications for volatile recycling in subduction zones. Geochim Cosmochim Acta 67:4179–4203

Sun M, Kerrich R (1995) Rare-earth element and high-field strength element characteristics of whole rocks and mineral separates of ultramafic nodules in Cenozoic volcanic vents of Southeastern British–Columbia, Canada. Geochim Cosmochim Acta 59:4863–4879

Sun SS, McDonough WF (1989) Chemical and isotopic systematics of oceanic basalts: implications for mantle composition and processes. In: Saunders AD, Norry MJ (eds) Magmatism of the Ocean Basins. Special Publication, vol 42. Geological Society, London, pp 313–345

Sykes D, Rossman GR, Veblen DR, Grew ES (1994) Enhanced H and F incorporation in borian olivine. Am Miner 79:904–908

Thompson JB (1978) Biopyriboles and polysomatic series. Am Miner 63:239–249

Tilley CE (1951) The zoned contact-skarns of the Broadford area, Skye: a study of boron–fluorine metasomatism in dolomites. Min Mag 29:621–673

Trommsdorff V (1983) Metamorphose magnesiumreicher Gesteine: Kritischer Vergleich von Natur, Experiment und thermodynamischer Datenbasis. Fortschr Miner 61:283–308

Trommsdorff V, Evans BW (1972) Progressive metamorphism of antigorite schist in the Bergell Tonalite Aureole (Italy). Am J Sci 272:423–437

Trommsdorff V, Evans BW (1974) Alpine metamorphism of peridotitic rocks. Schweiz Mineral Petrogr Mitt 54:334–352

Trommsdorff V, Evans BW (1980) Titanian hydroxyl-clinohumite—formation and breakdown in antigorite rocks (Malenco, Italy). Contrib Mineral Petrol 72:229–242

Trommsdorff V, López Sánchez-Vizcaíno V, Gómez-Pugnaire MT, Müntener O (1998) High pressure breakdown of antigorite to spinifex-textured olivine and orthopyroxene, SE Spain. Contrib Mineral Petrol 132:139–148

Trommsdorff V, Risold AC, Reusser E, Connolly JAD, Ulmer P (2001) Titanian clinohumite: ilmenite rod inclusions and phase relations, Central Alps. In: UHPM workshop. Waseda University, pp 84–85

Ulmer P, Trommsdorff V (1995) Serpentine stability to mantle depths and subduction-related magmatism. Science 268:858–861

Veblen DR (1991) Polysomatism and polysomatic series—a review and applications. Am Miner 76:801–826

Veblen DR (1992) Electron microscopy applied to nonstoichiometry, polysomatism, and replacement reactions in minerals. In: Buseck PR (ed) Minerals and reactions at the atomic scale:-TEM. Reviews in Mineralogy, vol 27. Mineralogical Society of America, Washington DC, pp 181–230

Wei CJ, Powell R (2003) Phase relations in high-pressure metapelites in the system KFMASH (K_2O–FeO–MgO–Al_2O_3–SiO_2–H_2O) with application to natural rocks. Contrib Mineral Petrol 145:301–315

Weiss M (1997) Clinohumites: a field and experimental study. PhD Thesis. ETH, Zurich, pp 168

Weiss M, Müntener O (1996) Crystal chemistry of titanian-clinohumite: implications for storage of HFSE in the mantle. In: Sixth VM (ed) Goldschmidt conference. Cambridge Publications, Heidelberg, p 665

White RW, Powell R, Phillips GN (2003) A mineral equilibria study of the hydrothermal alteration in mafic greenschist facies rocks at Kalgoorlie, Western Australia. J Metamorph Geol 21:455–468

Wirth R, Dobrzhinetskaya LF, Green HW (2001) Electron microscope study of the reaction olivine + H_2O + $TiO_2$$ titanian clinohumite + titanian chondrodite synthesized at 8 GPa, 1300 K. Am Miner 86:601–610

Wunder B, Schreyer W (1997) Antigorite: high pressure stability in the system MgO–SiO_2-H_2O (MSH). Lithos 41:213–227

Yamasaki T, Seno T (2003) Double seismic zone and dehydration embrittlement of the subducting slab. J Geophys Res Solid Earth 108:art. no. 2212

Yang JJ (2003) Titanian clinohumite–gamet–pyroxene rock from the Su–Lu UHP metamorphic terrane, China: chemical evolution and tectonic implications. Lithos 70:359–379

Yang JJ, Jahn BM (2000) Deep subduction of mantle-derived garnet peridotites from the Su–Lu UHP metamorphic terrane in China. J Metamorph Geol 18:167–180